Packaged Printed Multilayer Beamforming Microwave Components

Mostafa O. Shady

A Thesis

In

The Department

of

Electrical and Computer Engineering

Presented in Partial Fulfillment of the Requirements

For the Degree of

Master of Applied Science (Electrical and Computer Engineering) at

Concordia University

Montreal, Quebec, Canada

August 2023

Concordia University

School of Graduate Studies

This is to certify that the thesis prepared

By: Mostafa O. Shady

Entitled: Packaged Printed Multilayer Beamforming Microwave Components

and submitted in partial fulfillment of the requirements for the degree of

Master of Applied Science (Electrical and Computer Engineering)

complies with the regulations of the University and meets the accepted standards with respect to originality and quality.

Signed by the final examining committee:

Dr. Abdel Razik Sebak _____ Chair

Dr. Kejia Ding _____ Examiner

Dr. Abdel Razik Sebak _____ Examiner

Dr. Ahmed A. Kishk _____ Thesis Supervisor

Approved by _____

Dr. Zahangir Kabir, Graduate Program Director

August 10, 2023 _____

Dr. Mourad Debbabi

Dean, Gina Cody School of Engineering and Computer Science

Abstract

Packaged Printed Multilayer Beamforming Microwave Components

Mostafa O. Shady, MASc

Concordia University, 2023

Low-loss, compact, and high-frequency microwave devices are in high demand to fulfill the currently required communication systems specifications. Thus, the present work is devoted to the design and compactness enhancement of microwave components. Multilayer technology for printed circuits is utilized for maximum size reduction with artificial magnetic conductor (AMC) packaging to create a self-packaged/shielded system.

An electromagnetic band-gap (EBG) cell is presented to miniaturize the size by replacing the mushroom patch with a spiral unit that lowers the stopband center frequency by half compared to the patch in the same cell size. The principle of operation and parametric studies are discussed. Also, methods to enhance the stop bandwidth are discussed.

Microstrip line (MSL) multilayer power dividers with equal power division to ports in two different layers but different phase outputs are designed. A via less power transfer between the layers is realized by an elliptic slot on the common

thick ground plane, which transfers the power throughout the layers capacitively. Various slot and matching transformer shapes control the phase difference between the output ports and the input matching bandwidth. AMC packaging is used to suppress radiation losses and leakage. The realized power dividers achieve a phase difference from 0° to 180° ±6° with a matching input level below -15 dB within 21.8% bandwidth at center frequency 29.75 GHz.

Finally, a novel 4 × 4 multilayer Butler matrix (BM) is proposed, reducing the conventional size by more than twofold. The design eliminates crossover couplers, considerably enhancing compactness and isolation, and uses air MSL packaged by an AMC to suppress wave leakage and radiation loss. The design and performance of the building block components are provided. The BM operates from 27 to 31 GHz with a 0.6 ± 1.4 dB insertion loss and a phase imbalance of ± 8°. It achieves isolation better than 14 dB with a good matching level. The presented 4 × 4 BM concept can be extended to N × N BMs. A four-slot linear antenna array is connected to the BM. The measured and simulated radiation characteristics are compared and found to be in good agreement.

Acknowledgment

I would first like to thank my thesis supervisor Prof. Ahmed Kishk for his support and patience throughout the Master's program. He allowed me to work independently but steered me in the right direction whenever needed. I was always welcome in Prof. Kishk's office whenever I ran into trouble or had an inquiry about my research. I would also like to express my deep gratitude to my parents for supporting me while researching and writing this thesis.

Contents

List of Figures

List of Tables

List of Acronyms

AMC	Artificial Magnetic Conductor
BM	Butler Matrix
CPW	Coplanar Waveguide
EBG	Electromagnetic Bandgap
GCPW	Grounded Coplanar Waveguide
GW	Gap Waveguide
mmWave	Millimeter-Wave
MSL	Microstrip Line
OC	Open-Circuit
PCB	Printed Circuit Board
PEC	Perfect Electric Conductor
PMC	Perfect Magnetic Conductor
PRGW	Printed Ridge Gap Waveguide
RF	Radio Frequency
SIW	Substrate-Integrated Waveguide
TE	Transverse Electric
TEM	Transverse Electric Magnetic

Chapter 1

Introduction

1.1 Millimeter-Wave Technology

The millimeter-wave (mmWave) range appealed to academic and industrial applications due to its ability to achieve high data rates, low latency, and high capacity [1]. Older generations' data rates and system capacity cannot sustain the current increase in the number of users and data traffic generated by the current networks. As a result, mmWave frequencies and components emerged to fulfill the requirements due to their higher bandwidth and more compact components. The 5G mmWave starts at the 24.25 GHz range, with bands above at higher frequencies [2]. The high frequency allows high data rates to transfer in the range of Gbps [3], allowing faster communication and supporting various users simultaneously. Nevertheless, the listed advantages come at the cost of a shorter range of communication due to high atmospheric absorption levels at high-frequency levels, increasing the losses. This causes the optimum applications for mmWave technology to be short-range and indoor communications.

1.2 Traditional Printed Guiding Structures

1.2.1 Microstrip Line

Microstrip line (MSL) is the famous planar transmission line in RF and microwave circuits. It comprises a strip conductor on top of a dielectric substrate layer and a lower conductor, which serves as the ground plane [4], as shown in Figure 1.1(a). Its popularity and frequency of use come from being planar, having a low cost, compact size, and being simple to manufacture using various methods, with the most popular being the printed circuit board (PCB) version of a wire over a ground plane. It also tends to radiate as the spacing between the ground plane and strip line increases, so a substrate thickness of a fraction of a wavelength minimizes radiation without causing the strip width to be too narrow. The propagating mode is quasi-transverse electromagnetic (TEM) due to fringing fields in and above the dielectric substrate, lowering the effective dielectric constant more than the substrate dielectric constant. Radiation losses depend on the dielectric constant, substrate thickness, circuit geometry, and the frequency of operation. The lower the dielectric constant, the lower the concentration of energy in the substrate region, which leads to more significant radiation losses. Additionally, radiation losses become significant at high frequencies, causing the MSL to be unsuitable for mmWave bands. Another version is suspended MSL, which lowers the loss by suspending the substrate over the air, as shown in Figure 1.1(b). The air between the bottom of the substrate and the ground plane contains most of the electromagnetic power. Hence, the insertion loss of the MSL is reduced because air fundamentally has no dielectric loss compared to standard circuit board substrates.

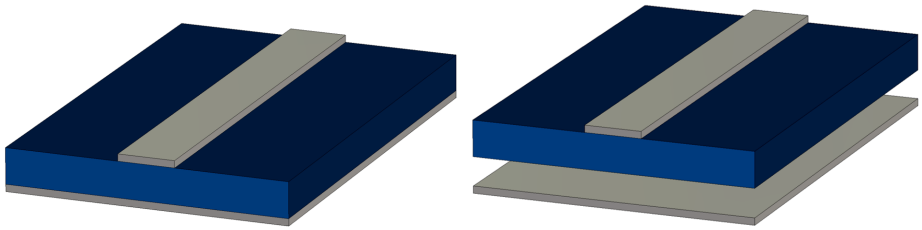

(a) (b)

Figure 1.1: (a) Microstrip line and (b) Suspended microstrip line

1.2.2 Coplanar Waveguide

Coplanar waveguide (CPW), in Figure 1.2(a), considered an alternative to MSL, places both the conducting strip and a pair of ground conductors on the sides of the strip on the same layer separated by a narrow gap. Also, bond wires could be placed to connect the ground planes [5]. Moreover, the gaps can be adjusted to the signal line width to offer more flexibility. The dimensions of the center strip, the gap, the thickness, and the permittivity of the dielectric substrate determine the effective dielectric constant, characteristic impedance, and attenuation of the line. The gap in the CPW is usually very small and supports electric fields primarily concentrated in the dielectric. The dielectric substrate thickness is usually about twice the gap width to concentrate the fields in the substrate area and minimize radiation. The CPW exhibits low dispersion due to minimal fringing fields in the air space. It has a zero cutoff frequency (suitable for wideband). However, the dominant propagating mode is also quasi-TEM. At higher frequencies, the field becomes less TEM and more transverse electric (TE), becoming dispersive. CPW is capable of lower-loss performance at much higher frequencies than MSL circuits but is harder to fabricate than MSL. Another variation is the grounded coplanar waveguide (GCPW), in Figure 1.2(b), used on PCBs as an alternative to MSL.

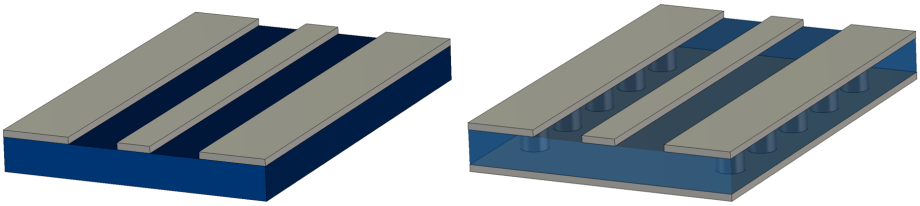

(a) (b)

Figure 1.2: (a) Coplanar waveguide and (b) Grounded coplanar waveguide

The gap between the strip and the ground is usually larger than the thickness of the substrate, making the GCPW field more concentrated between the strip and the substrate ground plane. This leads to the structure behaving like MSL, with vias connecting the ground planes for proper grounding. GCPW is less prone to radiation and has better isolation than MSL. Furthermore, the GCPW has fewer losses than the CPW, as a metal shield is used on the bottom to provide isolation from other circuits in lower layers [5]. However, the fabrication complexity and integration with other circuits are significantly increased.

1.3 Soft and Hard Surfaces

Soft and hard surfaces are metamaterials that artificially generate an anisotropic surface. Kildal described the definition of soft and hard surfaces in [6]. Soft surfaces have high-impedance in the direction of wave propagation and zero impedance in the transverse direction. Hard surfaces have zero impedance in the direction of propagation and high-impedance in the transverse direction. Thus, the soft surfaces are realized by transversely corrugated surfaces that suppress the propagation in the transverse direction, where the electric and magnetic fields are zero on such a surface, i.e., the power flux density becomes zero.

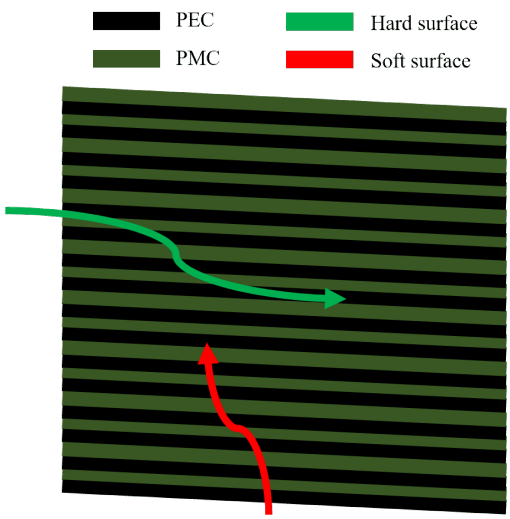

Figure 1.3: Soft and hard surfaces illustration

On the other hand, the hard surface eliminates the longitudinal field components, forcing the propagating wave mode to become TEM. The surfaces comprise transverse corrugation filled with dielectric or narrow successive strips of metallic conductors over a grounded dielectric of a thickness of a quarter-guided wavelength at stopband frequency. The overall structure can be homogenized and presented ideally as successive strips of perfect electric conductors (PECs) and perfect magnetic conductors (PMCs) with a period approaching zero, as depicted in Figure 1.3. The orientation of the corrugations will determine the direction of propagation and suppression of the wave [7].

1.3.1 Electromagnetic Band-gap Periodic Surfaces

Sievenpiper introduced the high-impedance surface in 1999 [8], realized by metal patches on a grounded substrate with metalized via-holes, often called a mushroom surface. The surface has a frequency band where no surface wave can propagate, similar to the soft surface. However, the mushroom surface suppresses surface

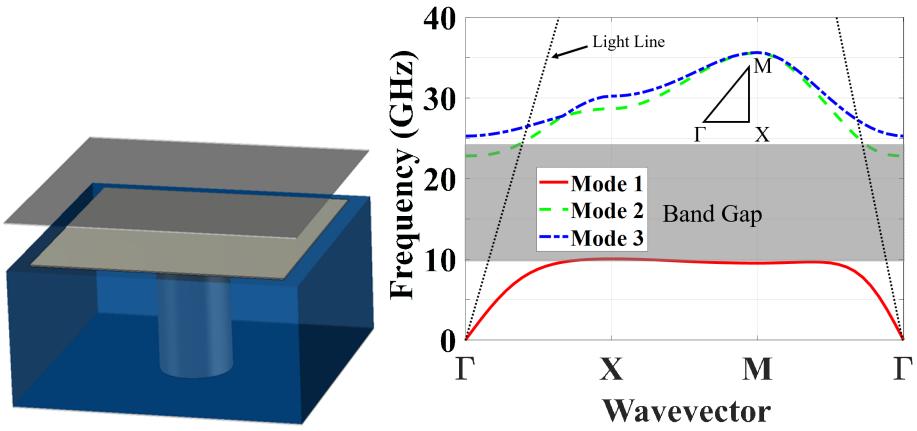

(a) (b)

Figure 1.4: EBG cell (a) Square patch cell structure and (b) Dispersion diagram

wave propagation in all directions at the surface, opposite to the soft surface, which prohibits wave propagation transverse to the corrugations only. The high-impedance surfaces are usually called electromagnetic band-gap (EBG) surfaces. The surface comprises periodic mushroom unit cells, shown in Figure 1.4(a), which are periodically repeated in the transverse and longitudinal axes. The eigenmode analysis is used to discover the propagating modes and their frequency bands to determine the band-gap, as shown in Figure 1.4(b). The wavevector is plotted with respect to the frequency for each mode, where **Γ**, **X**, and **M** represent phase values for the wavevector in tensor form. However, for symmetric unit cells, the one-dimensional analysis would be sufficient. The high-impedance surface could be employed in multiple applications, such as suppressing surface waves, reducing mutual coupling, and AMC packaging of microwave circuits.

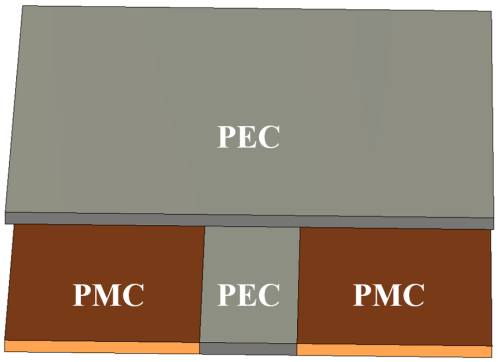

Figure 1.5: Gap waveguide ideal form

1.4 AMC Packaged Printed Guiding Structures

1.4.1 Gap Waveguide

The gap waveguide (GW) guiding medium was introduced in [9]. It integrates the soft surface inside the waveguide surrounding a metallic ridge with a parallel metal plate on top with a height of less than a quarter wavelength, as shown in Figure 1.5, illustrating the ideal case with PEC and PMC. In GW, the field travels in the air gap between parallel metal plates without requiring metal contact between both plates, simplifying the fabrication process. Also, the dominant mode of operation is quasi-TEM, mitigating the dispersion effects. Consequently, GW is a promising alternative to traditional guiding mediums for high-frequency applications. The printed practical form of this waveguide is the printed ridge gap waveguide (PRGW) [10–15], displayed in Figure 1.6. The wave is confined above the ridge, with the EBG cells suppressing leakage in the designed stopband region. This structure incorporates the EBG cells and the ridge on the same layer, requiring a transition to a traditional medium to feed the structure. An MSL transition is applied for its simplicity and coverage of the whole bandwidth [16].

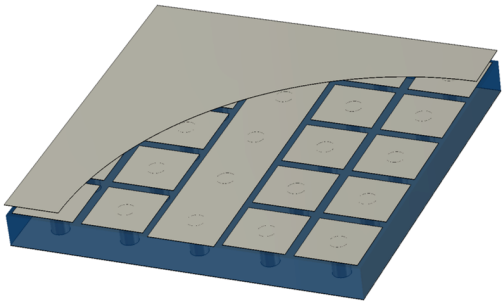

Figure 1.6: Printed ridge gap waveguide

1.4.2 AMC Packaged MSL

EBG cells could be used to AMC package MSL directly, as shown in Figure 1.7, eliminating the need for a transition [17]. A thin substrate separates the line from the EBG cells, keeping an air gap between the line and the upper ground. This air gap is supported by spacers around the edges of the circuit to ensure constant permittivity. The advantage of using an air gap is having a slightly wider bandwidth and lower dielectric losses. Furthermore, the AMC packaging of MSL affects the characteristic impedance based on the proximity of the AMC surface to the MSL. Thus, it can also be used to change the characteristic impedance to allow a wider line width to simplify fabrication and ease integration with other circuits. Alternatively, a low permittivity substrate could be used instead of the air gap to ensure a fixed height and simplify the integration process even further with other PCB circuits.

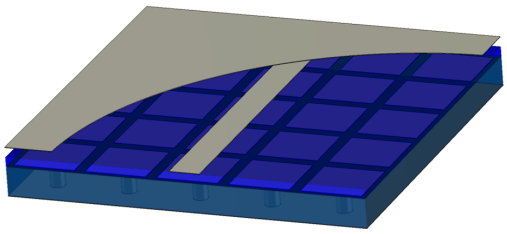

Figure 1.7: AMC packaged MSL

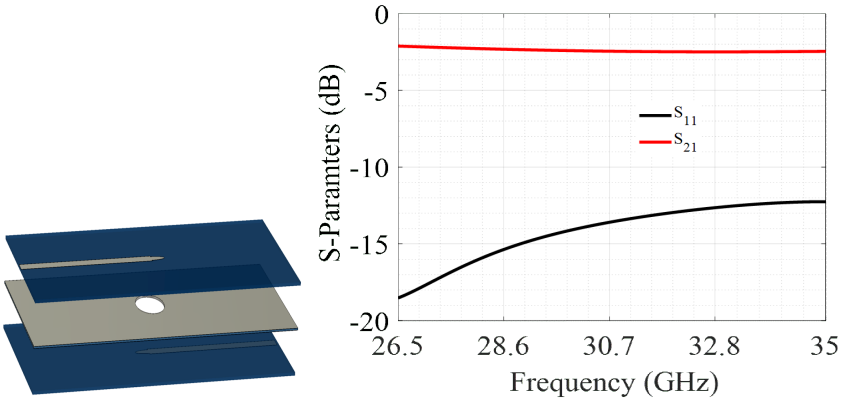

(a) (b)

Figure 1.8: MSL multilayer lines (a) Exploded view and (b) Scattering parameters

The major advantage of AMC packaging MSLs is its ability to solve radiation losses, surface waves, and cavity resonances for multilayer structures, especially at mmWave bands where radiation losses dominate. An example of a multilayer MSL structure operating at the Ka-band is displayed in Figure 1.8. It can be seen that the insertion loss is worse than 2 dB, with a high level of return loss all-over the bandwidth. Conversely, the AMC packaged version of the multilayer structure is depicted in Figure 1.9. The insertion loss is now better than 0.4 dB, and the matching is better than -20 dB over most of the bandwidth. Therefore, AMC packaging could be utilized to realize multilayer microwave components at mmWave bands using MSL technology to miniaturize the circuit components instead of relying on 3D printed or metallic structures.

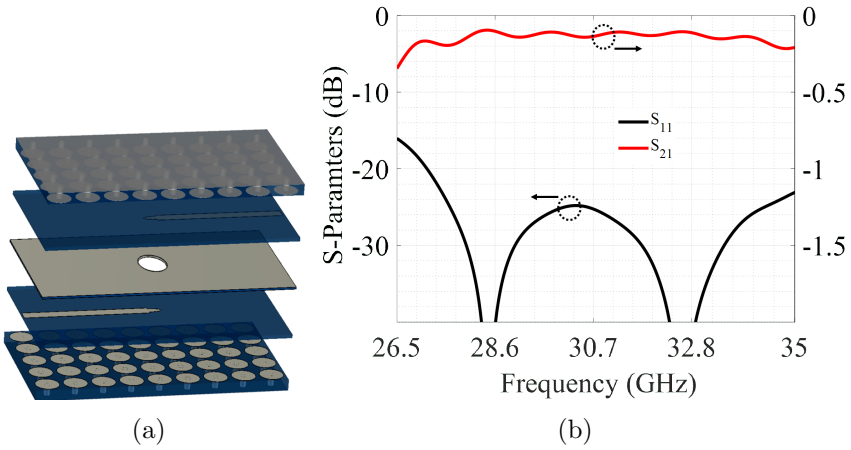

(a) (b)

Figure 1.9: AMC packaged MSL multilayer lines (a) Exploded view and (b) Scattering parameters

1.5 Objectives

The main objective of this thesis is to miniaturize printed microwave components for mmWave frequency band applications. A possible method is to design multilayer structures, as the thickness at such frequencies is negligible. Stacking multiple layers would not expand the overall size by a significant amount. However, radiation losses dominate at high frequencies using traditional guiding structures. Consequently, AMC packaging suppresses radiation and creates self-shielded multilayer structures. The first objective is to study the theory of operation of EBG cells and propose a new design to enhance the compactness of periodic structures. The second objective is to design microwave components based on the AMC packaged multilayer layout with a wideband of operation. The final objective is to present a simple layout for beamforming networks based on multilayer structures applicable to N $\times$ N sizes.

1.6 Thesis Organization

The thesis is divided into six chapters. The first chapter introduces the thesis and discusses mmWave technology, the printed guiding mediums used, and their characteristics. The second chapter reviews planar, multilayer, and AMC packaged microwave components found in the literature. Chapter three explains the EBG cell operation and proposes a new compact design that reduces the size by half. Chapter four presents a new multilayer power divider with equal power division and different output phases with AMC packaging. Chapter five presents an N $\times$ N multilayer Butler matrices (BMs) layout, and a 4 $\times$ 4 AMC packaged structure is designed based on these layouts. Finally, the last chapter summarizes the work done in the thesis and suggests further developments.

Chapter 2

Planar, Multilayer, and AMC Packaged Printed Microwave Components

This chapter briefly reviews microwave components found in the literature with planar and multilayer printed structures. Also, AMC packaged structures are presented where multilayer ones are uncommon in literature.

2.1 Planar Microwave Components

MSL planar microwave components have been used for decades due to their cheap and compact structures [18–22], as presented in Figure 2.1. They generally offer broadband operation at low frequencies with acceptable losses. A good example to present most of the microwave components is the BM in [21]. Combining quadrature 3-dB couplers, phase shifters, and a crossover coupler to construct the beamforming network. A two-section branch line type of coupler widens the

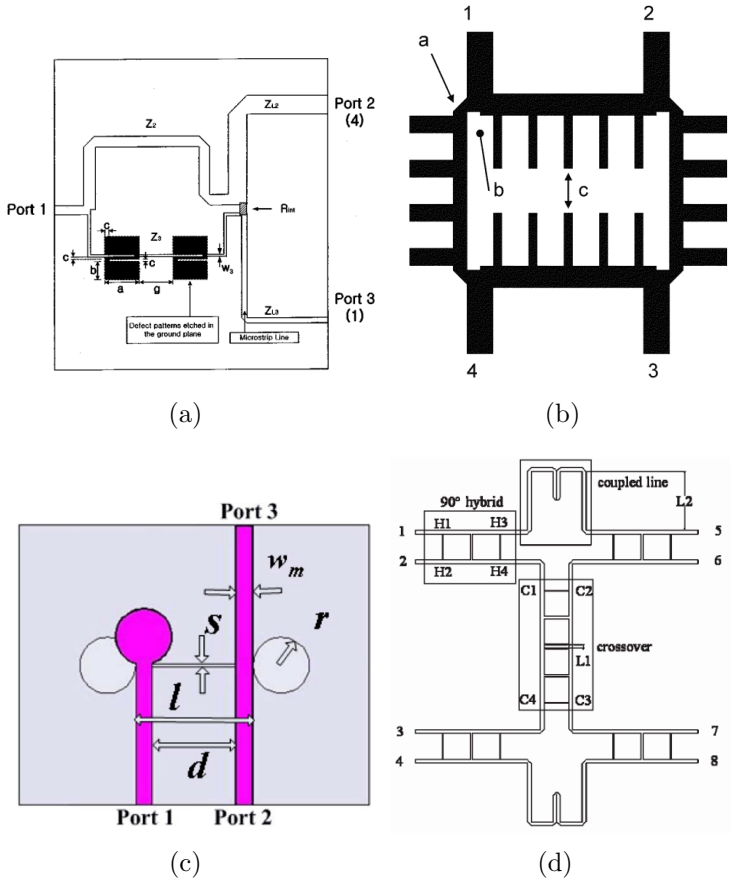

Figure 2.1: Planar microstrip microwave components (a) Unequal Wilkinson power divider [18], (b) Branch line coupler [19], (c) Power divider [20], and (d) BM [21]

bandwidth and decreases the amplitude ripple. The crossover coupler cascades the hybrid couplers and adjusts the interconnection length to optimize the matching. A Schiffman phase shifter [23] is used, with the coupled line length tuned to achieve the 45° phase shift. The return loss and isolation of the BM are better than 15 dB over the bandwidth 9-11 GHz, with an insertion loss of 0.7 $\pm$0.7 dB and $\pm$10° phase error. Multiple sections could be used for each component to achieve a better response [22], but at the cost of a larger overall size. Furthermore, planar microstrip microwave devices in the literature have similar characteristics, such as

a maximum operating range at Ku-band, high loss at higher frequencies, and a large size to achieve a better response.

2.2 AMC Packaged Planar Microwave Components

AMC packaging planar microstrip microwave components can significantly improve the transmission performance at mmWave frequencies by suppressing radiation losses. AMC packaged microwave components were designed in [24–28]. The overall structures are shown in Figure 2.2. All designs are similar and composed of three layers, with layer 1 containing the EBG cells, layer 2 acting as a spacer between the cells and the MSL, and layer 3 being the MSL where the wave propagates within. Alternatively, some designs have the line and EBG on the same layer. The crossover coupler combines a circular patch and ring resonator to achieve a wideband response, as presented in [29]. The quadrature hybrid coupler is a simple rectangular patch, which represents a multi-section $\lambda/4$ transformer for a branch line coupler that improves the overall response and bandwidth of the coupler. The filters are based on multi-section Chebyshev filtering. The scattering parameters of the couplers and filters show a stable and low-loss performance over a wideband at the Ka-band.

A complete beamforming network utilizing the AMC packaging was presented in [27] to demonstrate the benefits of such a configuration. The patch structure is used to realize the quadrature hybrid coupler and cascade two of them together to get the crossover couplers. A delay line is designed as a bent line loaded with open stubs and varying the dimensions to achieve the 45° or 0° phase shifts relative

to the crossover coupler over a wideband of operation. The BM's return loss and isolation level are below 15 dB within 28-33 GHz, with low phase and amplitude imbalance.

A comparison is carried out in Figure 2.3 between the components with and without AMC packaging. The insertion loss is reduced when a device is AMC packaged due to the suppression of radiation losses, where this improvement would be clearly seen in a beamforming network comprising multiple microwave components. The effect of AMC packaging multilayer structures would show a more significant effect regarding the insertion loss, even for single components in a circuit.

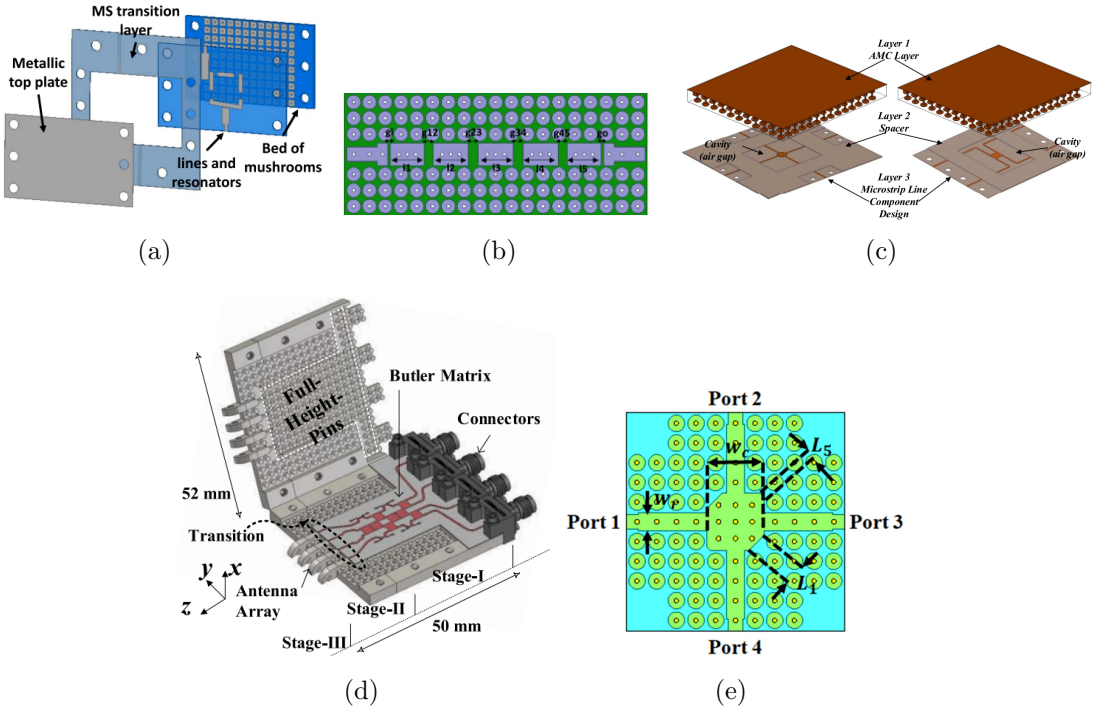

Figure 2.2: AMC packaged printed microwave components (a) Quadruplet filter [24], (b) Fifth order filter [25], (c) Crossover and quadrature hybrid couplers [26], (d) BM [27], and (e) Quadrature hybrid coupler [28]

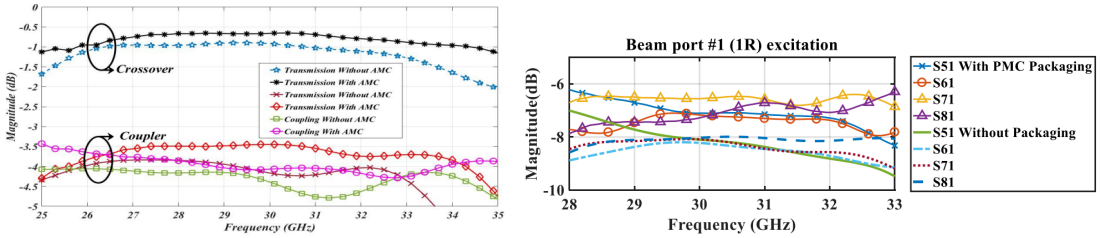

(a) (b)

Figure 2.3: Performance comparison with and without AMC (a) Couplers [26] and (b) BM [27]

2.3 Multilayer Microwave Components

MSL multilayer structures can be generally used at lower frequencies to reduce the circuit size and realize structures with aperture coupling. They are mostly realized at frequencies below the Ku-band, as the radiation losses increase significantly at higher frequencies. Multilayer microwave components were presented in [30–34] by employing aperture coupling, as shown in Figure 2.4. Elliptical slots are employed to couple the wave between the layers. Microstrip elliptical pads are placed directly underneath the slots to enhance the coupling and matching levels. The scattering parameters show a matching level below -15 dB for operation within 2.3-12.3 GHz for most components.

In [33], a multilayer BM was designed using crossover and slot-coupled directional couplers. A slot-coupled directional coupler splits the wave into both layers, with a rectangular coupling slot/microstrip. Cascading two of the slot directional couplers forms the crossover coupler, with only one used in the BM, and ports 6 and 7 are aligned at the end by crossing the two lines in different layers. The 45° phase shift is carried out by using delay lines relative to the crossover coupler. The return loss of the BM is better than 12 dB with stable transmission coefficients and a 5° phase error. Similar to what was presented, the multilayer MSL microwave

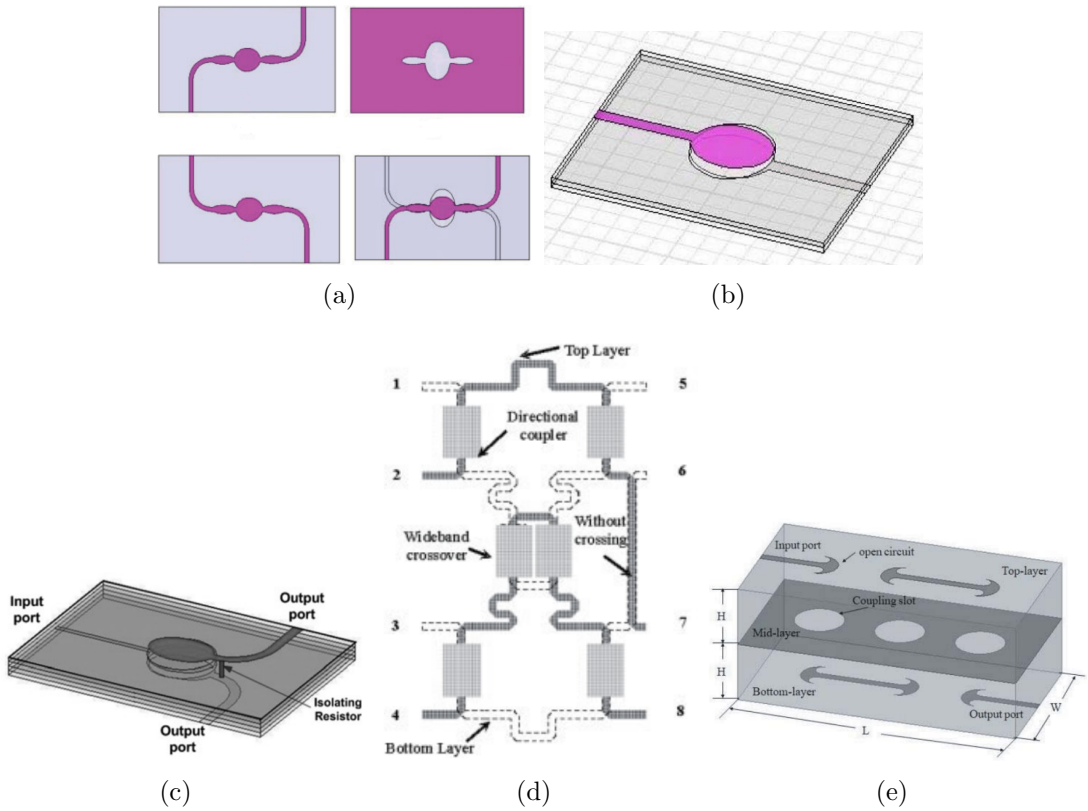

Figure 2.4: Multilayer microstrip microwave components (a) Aperture coupler [30], (b) Phase shifter [31], (c) Power divider [32], (d) BM [33], and (e) Filter [34]

components found in the literature all operated at lower frequencies.

2.4 AMC Packaged Multilayer Microwave Components

To mitigate the losses of radiation and design multilayer structures at high frequencies, EBG cells are used for packaging the structure, suppressing any leakage, and confining the wave inside the medium. A directional aperture coupler operating in the V-band was proposed in [35] using PRGW technology. In PRGW, the ridge is bounded by EBG cells in the top and bottom layers, suppressing any leakage and allowing operation at higher frequency bands. The PRGW multilayer quadrature hybrid coupler is presented in Figure 2.5. A substrate is placed between the two lines with five rectangular slots drilled and surrounded by metallic vias to act as a PEC and prevent wave leaking inside the substrate. The coupler operates in the 57-64 GHz frequency range with 0.5 dB amplitude variation and only 1° of phase error.

Another aperture coupler operating at the Ka-band was proposed in [36] using PRGW technology. The ridge line with the transformers, the coupling pad, and the slot used are depicted in Figure 2.5. It can be seen that the periodicity of the EBG cells was disturbed when the coupling pad was introduced on the ridge

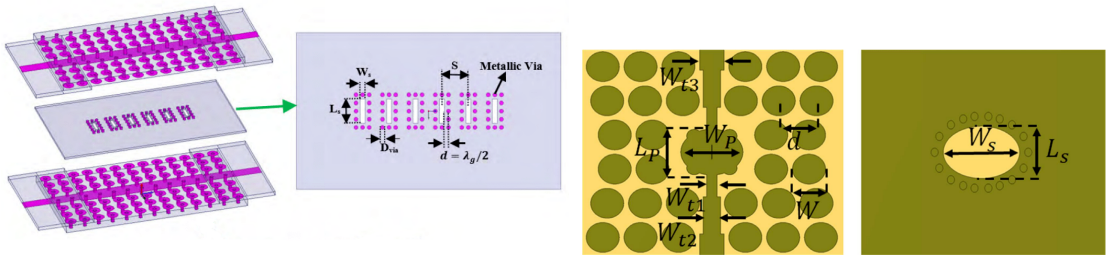

(a) (b)

Figure 2.5: AMC packaged printed aperture couplers (a) V-band coupler [35] and (b) Ka-band coupler [36]

due to sharing the same layer. Furthermore, matching transformers were needed to match the impedance of the line to the coupling pad. The dimensions of the slot can be varied to produce different coupling values in the range of 3-10 dB. The coupler displays return loss and directivity better than 10 dB for most of the bandwidth (25-37 GHz) with $\pm$ 1.5 dB and $\pm$ 6° amplitude and phase imbalances, respectively.

2.5 Summary

Microstrip printed technology has been utilized to realize multiple microwave components in both planar and multilayer layouts. AMC packaging is used to suppress radiation and allow operation at mmWave bands. Planar AMC packaged microwave components are commonly found in the literature instead of multilayer AMC packaged ones. The planar packaged designs consume a large network size to implement, while the unpackaged multilayer designs suffer high radiation loss at higher frequencies. This thesis aims to realize multilayer AMC packaged components operating at the Ka-band with compact size. The thesis focuses on designing a miniaturized multilayer beamforming network by eliminating the requirement for a crossover coupler and designing components that could be implemented in a compact layout.

Chapter 3

EBG Cell Size Reduction by Elongating Surface Current Path

EBG cells can package microwave circuits, suppress surface waves, or even be integrated inside some waveguide types to enhance compactness and reduce losses. The EBG cell parameters determine the stopband where wave propagation is suppressed [7]. Many empirical studies have been conducted to define a standard design procedure to enhance the bandwidth [37, 38]. The conventional EBG cell design is best utilized for applications operating at the mmWave band [39]. At lower frequency bands, the dimensions of the EBG cell are exceedingly significant, thus removing the compactness and integration ability. For height reduction, a mushroom type is used in printed circuit technology. As a result, the line and surface currents increase, shifting the operating frequency down and improving the stopband. The original bed of nails structure, about a quarter of wavelength height, provides a 2:1 bandwidth. The printed EBG cell of the mushroom has a slightly smaller bandwidth. A limited amount of work has studied the EBG cell and proposed methods to improve the bandwidth [40]. Little effort has been em-

ployed to reduce the size and improve the bandwidth [41, 42]. Thus, discussions on the mushroom EBG cell patch effect on the bandwidth and its theory are presented here. Subsequently, methods to shift down the stopband and a proposed spiral EBG cell design are presented in detail.

3.1 Traditional EBG Cells

The traditional mushrooms of a square or circular patch are displayed with their current distribution in Figure 3.1 and their dispersion diagram. The EBG cells are printed on Rogers RT6002 (thickness = 1.524 mm) with period = 3.2 mm, patch radius = 1.4 mm, pin radius = 0.4 mm, and gap height = 0.508 mm. The surface current distribution shows that the square patch has a more extended surface current path due to its larger area. Thus, its operating frequency is lower with a broader bandwidth, utilizing the concept of a longer current path. Also, the surface current starts at the via and extends to the edges. Consequently, shifting the via to the edge will offer a longer current path to the edges and shift the stopband down, as shown in Figure 3.2.

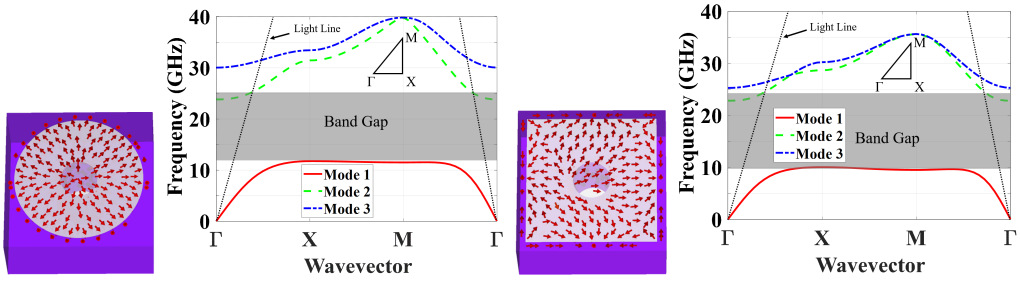

Figure 3.1: Traditional mushroom EBG cells (a) Circular patch with surface current distribution (second mode), (b) Circular patch dispersion diagram providing band-gap 11.7-25.1 GHz (72.8%), (c) Square patch with surface current distribution (second mode), and (d) Square patch dispersion diagram providing band-gap 10-23.8 GHz (81.6%)

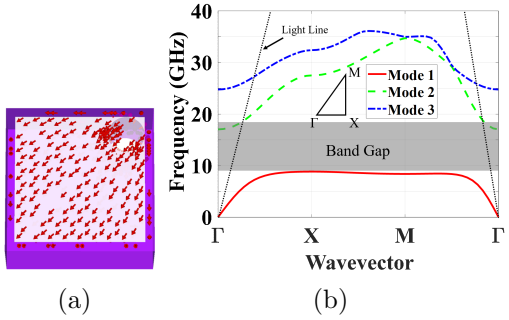

Figure 3.2: Square patch with shifted via EBG cell (a) Square patch with shifted via structure with surface current distribution (second mode) and (b) Dispersion diagram providing band-gap 8.8-18.4 GHz (70.5%)

3.2 EBG Cell Size Reduction

The EBG of a spiral strip would offer a longer current path and shift the frequency down [43, 44]. With the same EBG cell size, the square patch is shaped as a one-turn spiral starting from the EBG center by introducing a 0.2 mm U-shaped slit with the via shifted to the edge to offer the longest current path, as shown in Figure 3.3. It should be stated that the spiral strip width is constrained by the via diameter at its starting position due to the fabrication constraints that require

a specific via diameter with respect to the substrate thickness. The spiral shifts the stopband center frequency by half but with a smaller bandwidth, and another stopband is found between 16.6-19.9 GHz. Looking at the current distribution, one would notice that the current forms a ring in the azimuthal direction rather than the radial path in the solid patches (circular or square).

Due to fabrication constraints, the spiral strip width is designed to be wide, with a minimum separation between the turn edges of 0.2 mm. It was preferred to maximize the area to offer a wider stopband. However, a lower shift could be achieved by applying more turns with a narrower strip at the cost of a narrower stopband. The spiral cell is scaled down to shift the starting stopband up to correspond to the lower frequency of the square patch, as depicted in Figure 3.4. The spiral, square patch with shifted via, and traditional mushroom EBG cells are compared in Table 3.1 regarding bandwidth and size calculated with respect to the lower frequency. The spiral EBG cell offers a 30% size reduction compared to the square patch EBG cell. Such a reduction would make it more suitable for packaging and circuits with many discontinuities.

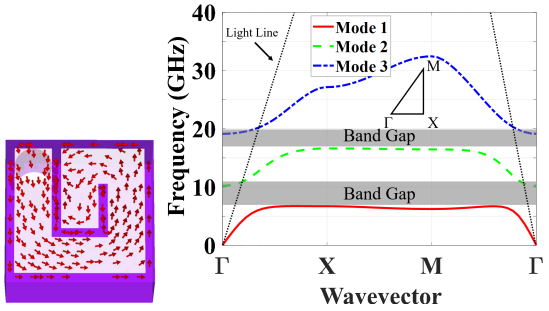

(a) (b)

Figure 3.3: Spiral-shaped EBG cell (a) Spiral patch with surface current distribution (second mode) and (b) Dispersion diagram providing two narrow band-gaps 6.7-11.2 GHz (50.2%) and 16.6-19.9 GHz (18%)

Table 3.1: Comparison between traditional patches and spiral-shaped EBG cells

6 × 6 EBG cells	Stopband	Size ($\lambda_0{}^2$)
Circular patch	11.7-25.1 GHz	0.75 × 0.75
Square patch	10-23.8 GHz	0.64 × 0.64
Square patch with via shifted	8.8-18.4 GHz	0.56 × 0.56
Spiral shape	10.2-16.6 GHz 27-32.9 GHz	0.45 × 0.45 1.19 × 1.19

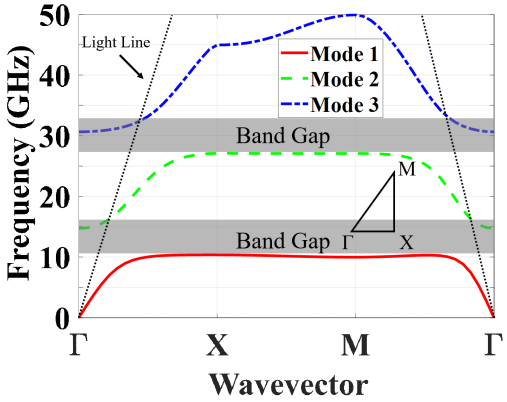

Figure 3.4: Dispersion diagram of the scaled spiral EBG cell providing two narrow band-gaps 10.2-16.6 GHz (47.7%) and 27-32.9 GHz (19.6%) (period = 2.2 mm, pin radius = 0.23 mm, gap height = 0.254 mm, and thickness = 0.762 mm)

3.3 Summary

The operation of the EBG cell and the parameters affecting the band-gap have been examined in this chapter. By repositioning the via to maximize the current path, it is possible to shift down the band-gap of the conventional cell. Moreover, to reduce the operating frequency while keeping the same compact construction, a spiral-shaped EBG cell with its via placed at the edge has been proposed to lower the operating frequency. The spiral EBG cell is substantially smaller than a standard EBG cell with the same starting stop-band frequency.

Chapter 4

Packaged In-Phase/Out-of-Phase Printed Multilayer Power Dividers

Power dividers with different output phases and/or amplitudes could be needed for many applications, such as feeding antenna array systems to obtain a beam directed toward a certain direction [45]. Such dividers in multilayer structures are rarely found in the literature and are hard to design due to the difficulty of phase-matching different layers [46]. As a result, multilayer power dividers with equal power division and different output phases are proposed using AMC packaged inverted MSL technology.

4.1 Multilayer Power Divider Design

The layout of the proposed power divider is presented in Figure 4.1. The overall size of the structure is $1.46\lambda_g \times 0.81\lambda_g$. Packaging substrates (1 and 5) and

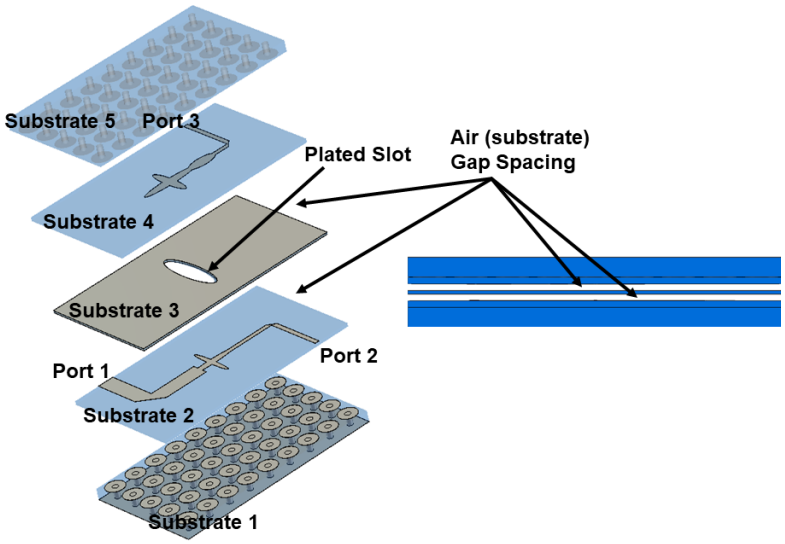

Figure 4.1: Exploded and cross-sectional views of the proposed MSL multilayer AMC packaged power divider

inverted MSLs (2 and 4) are printed on Rogers RT6002 with thicknesses of 0.762 mm and 0.254 mm, respectively. The slot, on Rogers RO3003 substrate 3 of 0.127 mm thickness, is cut to have a hollow opening by metalizing its inner boundaries to be electrically connected to the top and bottom substrates' conductor cladding. Thus, the whole substrate acts as a thick, solid conductor. All the substrates are stacked, as shown in Figure 4.1 with air gaps of 0.254 mm between the slot and MSL layers. The uniformity of the air gap thickness is maintained by inserting dielectric spacers. With this arrangement, the MSL propagates on an aired substrate. The coupling between the two layers of the MSLs is through elliptic pads (ellipses 2 and 4) around the slot. Ellipses 1-5 are used to achieve the required matching and output phase difference.

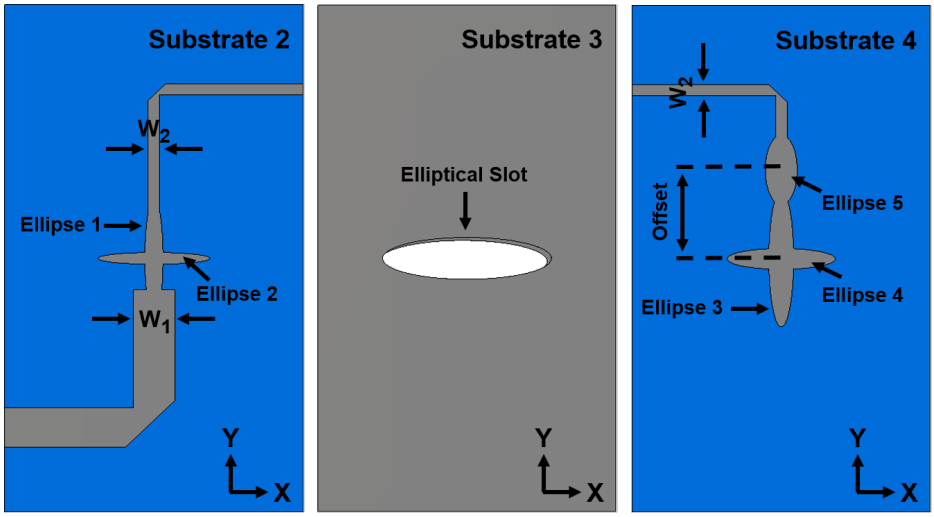

(a) (b) (c)

Figure 4.2: Power divider parameters (a) Substrate 2, (b) Substrate 3, and (c) Substrate 4

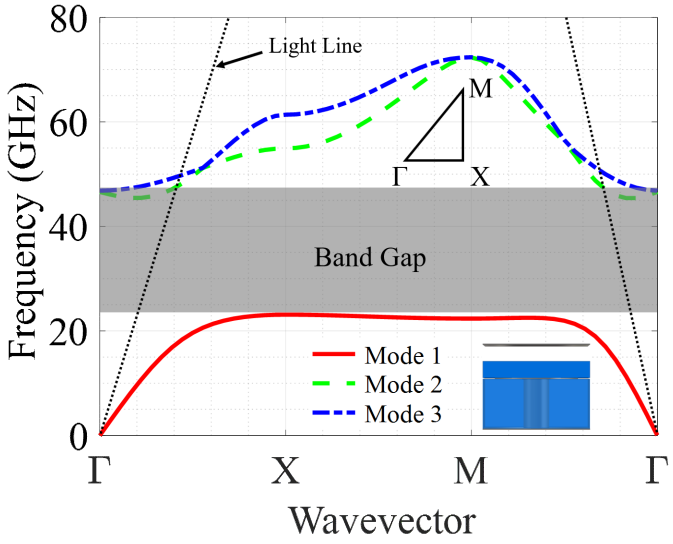

Figure 4.3: Dispersion diagram of the AMC cell

Table 4.1: Power dividers dimensions for different phase difference

Parameter (mm)	0	$\pi/2$	π
Ellipse 1 (r_x, r_y)	0.32, 0.65	0.25, 1.72	0.38, 3
Ellipse 2 (r_x, r_y)	2.28, 0.3	1.53, 0.17	1, 0.18
Ellipse 3 (r_x, r_y)	0.43, 0.82	0.34, 1.97	0.38, 2.6
Ellipse 4 (r_x, r_y)	1.17, 0.6	1.48, 0.3	1.12, 0.34
Ellipse 5 (r_x, r_y)	0.31, 0.9	0.43, 1.01	0.53, 0.75
Slot (r_x, r_y)	2, 0.51	2.32, 0.61	3.51, 0.5
Offset	0.98	2.6	1.58

The proposed structure can provide output phase differences ranging from 0° to 180°. The parameters affecting the matching and phase output of the power dividers are shown in Figure 4.2. The AMC is designed to cover the operating bandwidth to suppress any wave leakage. The dispersion characteristics indicating the band-gap of the AMC are presented in Figure 4.3. Initial line widths with characteristic impedances close to 50 Ω and 100 Ω for AMC packaged MSL can be calculated using the empirical formulas in [37]. In-phase, quadrature, and out-of-phase (0-, $\pi/2$-, and π-phase) power dividers are designed with their parameters listed in Table 4.1 with W_1 = 1.15 mm (48.5 Ω) and W_2 = 0.32 mm (93.2 Ω) for all dividers. The three different power dividers are designed and simulated, with their responses depicted in Figure 4.4. The power dividers display a return loss of better than 15 dB over 21.8% bandwidth with low phase variation. The complete structure is compact and packaged to shield the circuit from electromagnetic interference and prevent leakage through radiation. These types of power dividers can also be designed using PRGW technology and removing two substrates.

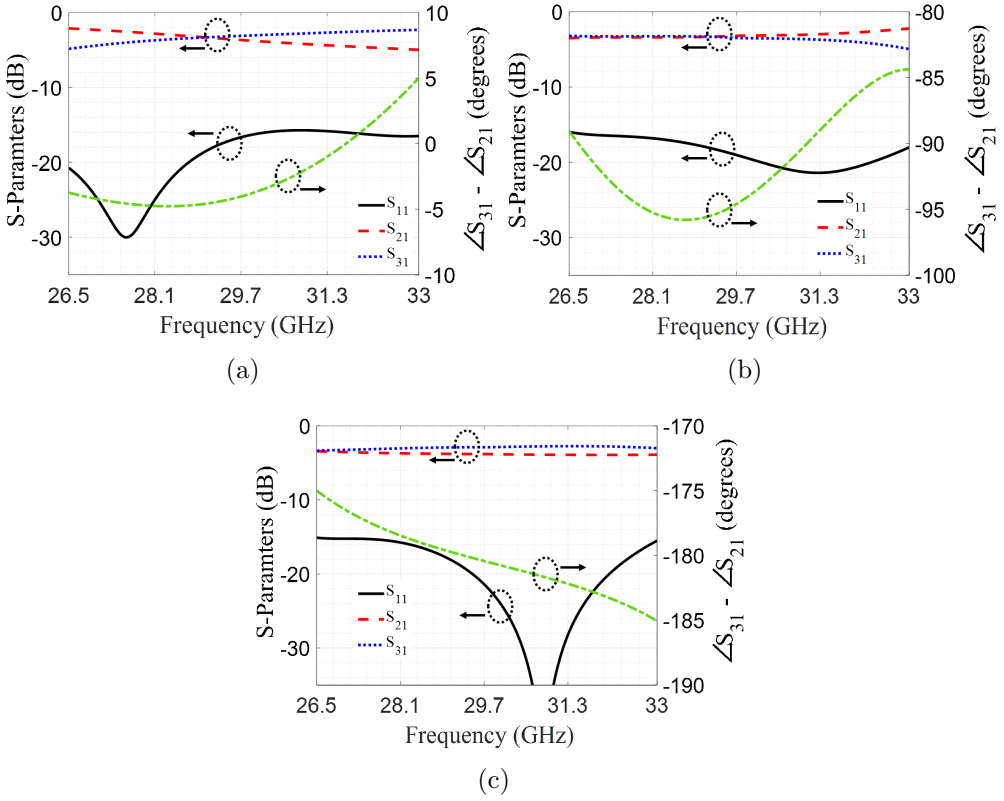

Figure 4.4: Realized multilayer power dividers responses (a) In-phase, (b) Quadrature, and (c) Out-of-phase

A parametric study of all the parameters affecting the power divider is conducted to show more depth behind the design structure. The values of the $\pi/2$ divider from Table 4.1 are used, and each parameter is varied while keeping the others fixed. The parameters of the slot and offset are varied in Figure 4.5. For the slot's major radius (r_x), values close to $\lambda_g/4$ display a good matching level and can also vary the phase difference and power distribution. Varying the minor radius (r_y) within reasonable values affects the phase imbalance. The offset of Ellipse 5 affects the matching level, phase, amplitude imbalance, and phase stability. The amplitude stability could be improved and phase shifted with an offset less than < 3 mm, however, the matching level must be improved with another parameter.

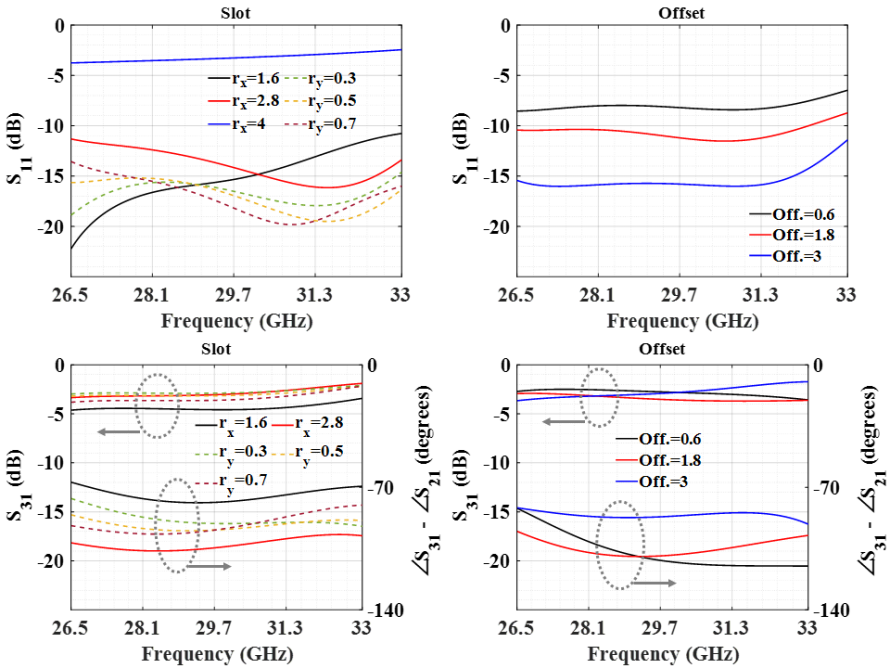

Figure 4.5: Effect of the slot and offset parameters on the frequency response

Figure 4.6 shows the effect of varying ellipses 1 and 2 radii. All the parameters have a significant effect on the matching level and power distribution. However, the radii perpendicular to the direction of propagation (r_x) have an effect on the phase and its imbalance. The effects of ellipses 3 and 4 are studied in Figure 4.7. The minor radius (r_x) has a severe effect on the matching level, while the major radius (r_y) controls the phase difference between the outputs. The parameters of ellipse 4 have a slight effect on the amplitude imbalance and matching level. Finally, the minor radius (r_x) of ellipse 5 affects the matching level, while the other responses are slightly changed, as shown in Figure 4.8.

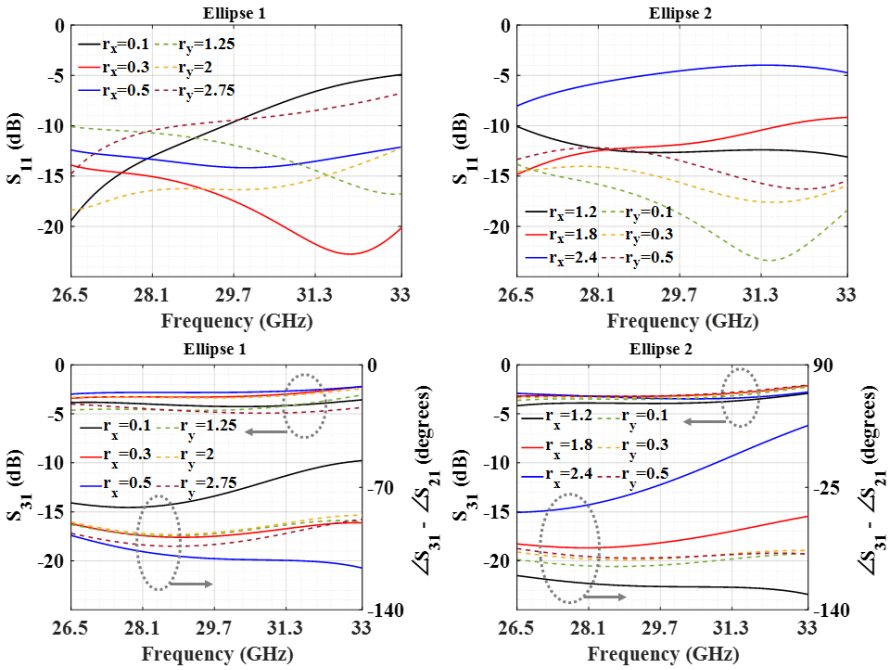

Figure 4.6: Effect of ellipses 1 and 2 radii on the frequency response

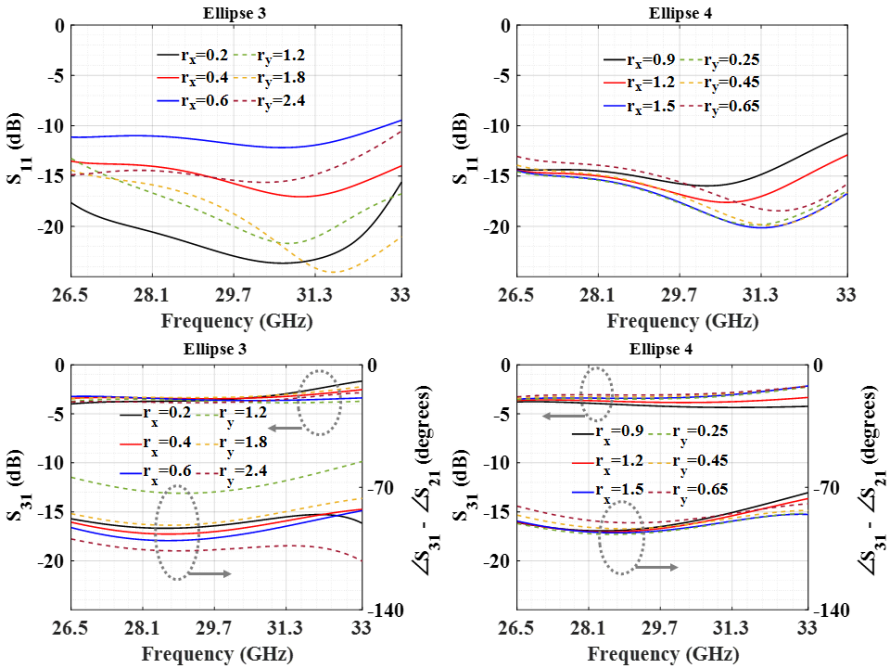

Figure 4.7: Effect of ellipses 3 and 4 radii on the frequency response

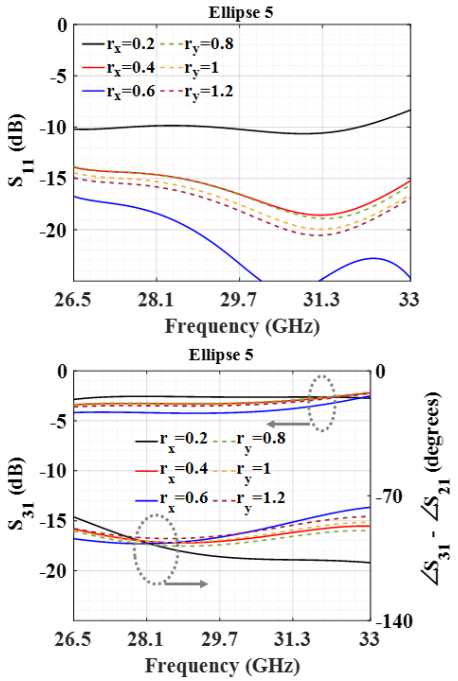

Figure 4.8: Effect of ellipse 5 radii on the frequency response

4.2 Summary

This work has presented MSL multi-layer power dividers with wideband operation in the Ka-band. The power divider layout could be modified to achieve phase differences ranging from in- to out-of-phase output ports. AMC packaging has been used to suppress radiation loss. The power dividers presented a good matching level and stable performance over their operating bandwidth.

Chapter 5

Compact 4 × 4 Multilayer Butler Matrix with Four-Slot Array

The proposed work combines multilayer MSL technology with AMC packaging to propose a compact beamforming network with suppressed radiation loss. A novel multilayer BM design that could be applied to any N × N BM is proposed, reducing the size by half. A multilayer wideband transition is designed for the wave to traverse through different layers with optimum performance. The 45° phase shift is achieved using a compactly designed delay line with a flat response. Different levels of phase shift can easily be obtained using the same structure with slight alterations of the component parameters for possible use with higher orders of BM. AMC packaging is used for the air MSL to suppress leakage and radiation loss. Also, AMC backed the radiating slots to eliminate direct back radiation from the radiating slot antennas. Thus, the design is self-packaged/shielded with a compact size and is suitable for printed circuit boards operating at the 5G mmWave bands. The system achieves stable, low-loss performance with high isolation and matching levels at the center frequency of 29 GHz with 13.8% bandwidth.

5.1 Multilayer Butler Matrices Layouts

An N × N traditional BM, where N = 2^n (n > 1), consists of $C_n = n2^{(n-1)}$ couplers, P_n = (n−1)$2^{(n-1)}$ phase shifters, and $X_n = 2X_{(n-1)} + 2^{(n-1)}(2^{(n-1)}\text{-}1)$ crossovers [47–49]. The BM feeds N-antenna elements to direct the beam toward two sets of beams (left side and right side sets mirroring each other around the center of the antenna ports, equally spaced by a distance d and uniformly excited in magnitude). The beam directions start from around the center, alternating between the left and right $\theta_B = \pm \sin^{-1}(\lambda d(2B-1)/2N)$, $B = 1, 2 \ldots (n+1)$ [50]. The phase difference between the antenna ports is $\phi_B = \pm\pi\ (2B-1)/N$ [51].

As the BM order increases, the structure's complexity increases and occupies significant space. Furthermore, multi-stage matching transformers are required to design a beamforming network with a wideband of operation and acceptable response, thus expanding the size further. Observing the layout of the conventional BM in Figure 5.1, one can see a mirror symmetry between the left and right sides of the BM. One method to reduce the size is by rearranging every two diagonal hybrids separately and aligning them horizontally, representing two inputs and two outputs, as shown in Figure 5.2. Folding the structure over the midline creates a compact BM without crossover couplers. The layout now consists of two separate layers with two input and two output ports each. In the sketches provided, T_δ represents a transition between two layers with a phase delay δ. Thus, T_{45° represents the transition between both layers, providing a 45° phase delay. This configuration eliminates the requirement for a crossover coupler, reduces the size significantly, and improves the isolation between ports. Also, the beamforming network length is effectively reduced to half, and now two layers containing pairs of couplers are stacked on top of each other instead of being side by side.

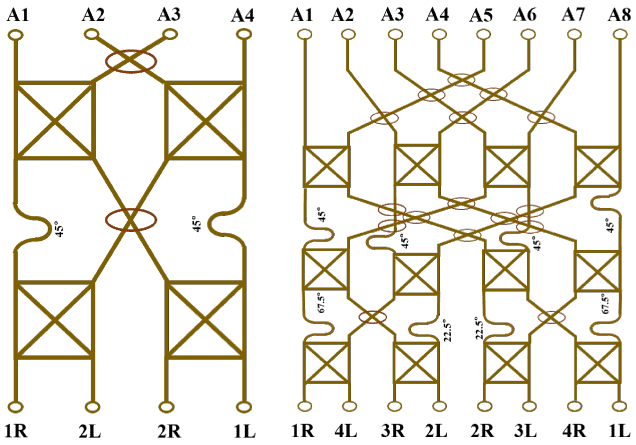

(a) (b)

Figure 5.1: Conventional sketch of (a) 4 × 4 BM and (b) 8 × 8 BM

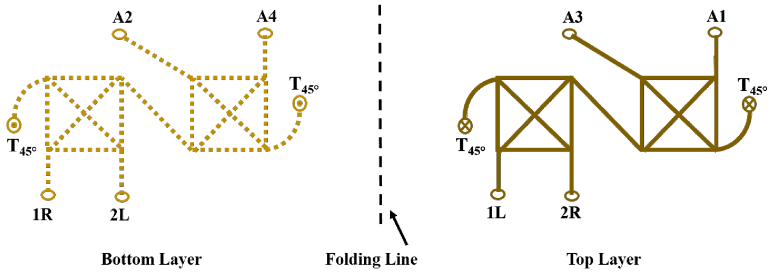

Figure 5.2: Sketch of folded 4 × 4 BM layout

Another alternative layout for the 4 × 4 BM is to have each diagonal coupler pair in one layer, as shown in Figure 5.3(a), with each pair with two inputs and two outputs following each other vertically in two different levels. Then, slide each pair to be aligned and following each other, and stack the top and bottom pairs, as shown in Figure 5.3(a). Like the folded layout, the multilayer transition T_{45° joins the two layers. This layout reduces the width by half and eliminates the need for crossover couplers. This format could be easily expanded to the 8 × 8 BM using the same procedure above to reach the sketch given in Figure 5.3(c). This sketch indicates that the crossover couplers still exist but are reduced by 12 crossovers

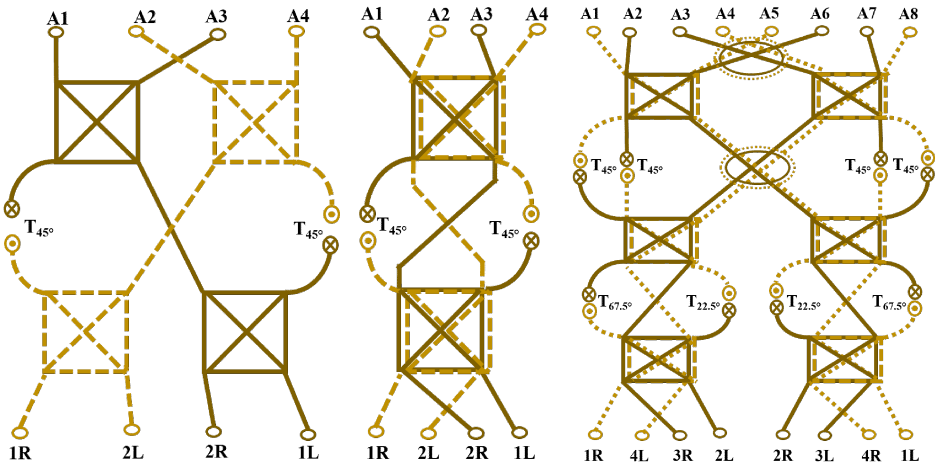

(a) (b) (c)

Figure 5.3: Alternative BM sketches (Bottom layer dashed and top layer solid) (a) Expanded 4 × 4 BM, (b) Top and lower level slid to be stacked on top of each other, and (c) Compact 8 × 8 BM

from the conventional layout, Figure 5.1(b), to Figure 5.3(c). However, the size is reduced to half. The same concept could be applied to any N × N BM, reducing its size by half.

5.2 Folded Butler Matrix Assembly

The folded 4 × 4 BM layout is selected to verify the multilayer concept at the mmWave band. Each component required is analyzed and designed individually. Finally, the components are integrated to form the folded layout. An air microstrip technology is employed as the guiding medium, with AMC packaging used to suppress radiation loss and create a self-shielded/packaged structure.

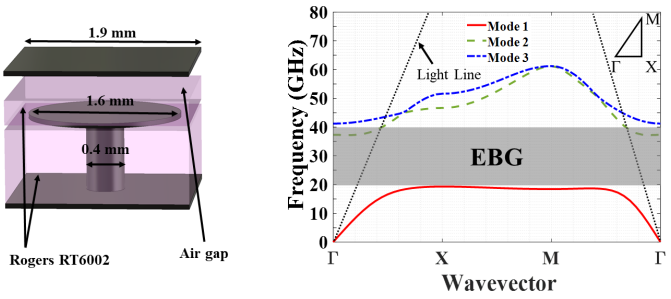

Figure 5.4: EBG cell and its dispersion diagram

5.2.1 EBG Packaging

The AMC packaging is realized using a periodic structure of mushrooms called cells, creating an EBG that suppresses wave propagation within a certain bandwidth. They exhibit high-impedance within the EBG, thus eliminating radiation loss, surface waves, and cavity resonance. A periodic EBG structure is placed beneath the MSL, ensuring wave suppression in longitudinal and transverse planes. A mushroom cell with a circular patch forms the high-impedance surface. The band-gap is determined by the cell parameters and permittivity of the supporting substrate [7]. The dimensions of the EBG cell are as follows: cell size = 1.9 $\times$ 1.9 mm^2, via diameter = 0.4 mm, and patch diameter = 1.6 mm. The EBG cell is printed on Rogers RT6002 (ϵ_r = 2.94) with a thickness of 0.762 mm. The substrate supporting the MSL is Rogers RT6002 with 0.256 mm thickness and is placed on top of the mushroom surface. An air gap of 0.256 mm between the MSL and its ground plane, supported by spacers, is selected as the propagation medium to increase the bandwidth and reduce dielectric losses. The dispersion diagram of the EBG cell is presented in Figure 5.4, showing the stopband of 19.3-40.8 GHz. The TE waves before the light line are leaky waves, propagating within a finite bandwidth. Thus, this region could be considered within the stopband. However, operation at the stopband limits is not recommended due to the finite magnetic

conductivity of the cells.

5.2.2 Quadrature Hybrid Coupler

A rectangular patch is used to realize a miniaturized hybrid coupler operating at the mmWave band [52, 53]. The patch represents a multi-section of $\lambda_g/4$ transformer for a branch line coupler to offer a wider band of operation with a better overall response. Furthermore, the packaged coupler is loaded with matching steps to enhance performance. The overall coupler structure and its performance are presented in Figure 5.5. The packaged line width used is 0.8 mm, with an impedance close to 50 Ω [37]. The length and width of the coupling patch are 4.7 mm, which is about $\lambda_g/2$ at the center frequency (29 GHz). The return loss and isolation of the structure are below 15 dB for most of the bandwidth (26-32 GHz), offering 20.6% of operation with low phase and amplitude variation. More complicated patch structures could be designed with less compact sizes to increase the bandwidth or improve the overall performance [14]. However, it was preferred to design compact components with the least amount of discontinuities to confine the components closely together.

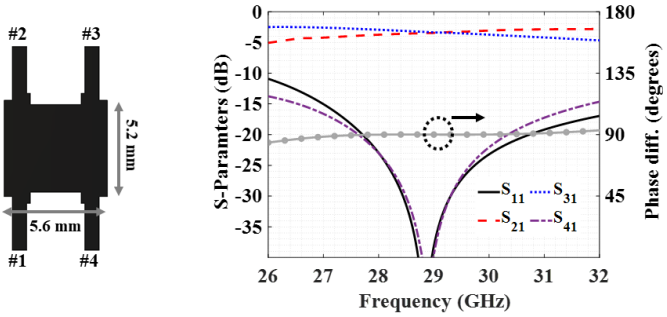

Figure 5.5: Quadrature hybrid coupler design and performance

5.2.3 Multilayer Transition

To transfer the power between different MSLs in two different layers, a simple transition is designed using a circular or elliptical slot on the common ground plane of thickness 0.127 mm between the propagating mediums (air medium) of the lines ending at the slot. A slot is drilled in the middle of the ground plane to allow the wave to propagate between the layers. A matching pad is placed in both layers perpendicular to the slot to enhance the coupling and matching levels. The layout of the optimized multilayer transition and its performance are presented in Figure. 5.6. The slot radius (r) is varied, as it has the most significant effect on the matching level of the transition. The transition possesses high-level insertion loss, worse than 2 dB over the whole bandwidth, even with a good matching level, indicating a high level of radiation loss.

By AMC packaging the transition, radiation losses are suppressed, and the boundary backing the line is changed from an open boundary to a magnetic conductor boundary, improving the insertion loss and matching levels. The resultant design and its response with various slot radii (r) are shown in Figure 5.7. The matching level can now be below -20 dB, and insertion loss better than 0.2 dB can be achieved over the whole bandwidth. Furthermore, a wider band of operation could be achieved by applying more matching transformers and/or slots. However, a non-coherent behavior against frequency is observed for the phase difference between the transition and a single-layer straight line of the same length.

A multilayer transition is employed on each side of the 4 $\times$ 4 BM. This orientation allows the two lines in the middle of the conventional BM to cross at two different layers, eliminating the requirement for a crossover coupler. Compared to the crossover coupler, the multilayer transition presents a better matching level

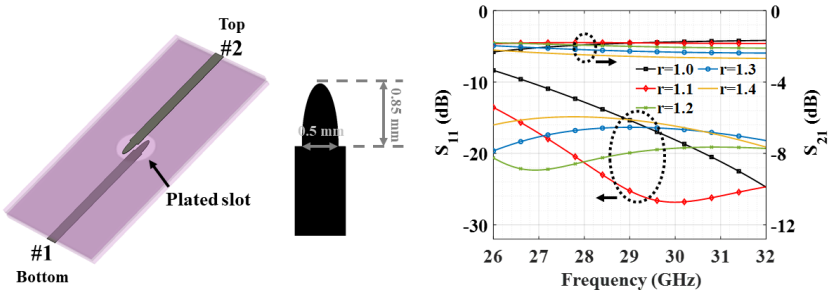

Figure 5.6: Effect of the slot radius (r) on the MSL multilayer transition performance

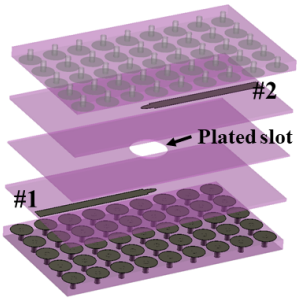

(a)

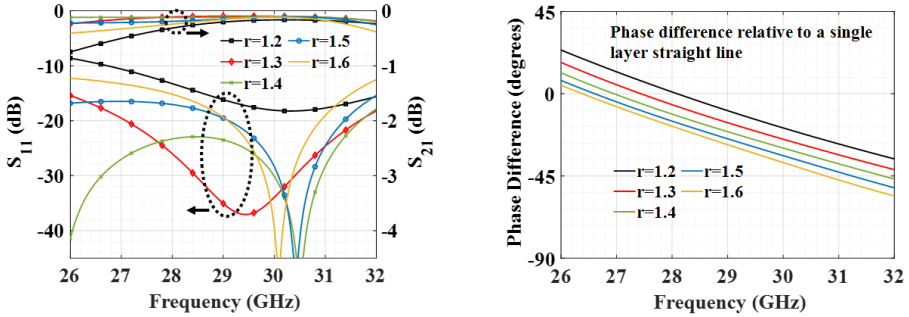

(b)

Figure 5.7: MSL transition packaged with AMC (a) Exploded view and (b) Effect of the slot radius (r) on the S-parameters and phase difference

and insertion loss over a wider band of operation with less complexity and size. Furthermore, crossing lines in different layers allows the isolation level to be theoretically infinite, as opposed to the crossover couplers, which typically have a level of around 15 dB.

5.2.4 Stub-Loaded Connecting line

As the multilayer transition now allows the split signal to propagate in two layers, a simple connection between the output of the coupler and the next stage can be made without requiring a crossover coupler. A very compact tilted line is designed in Figure 5.8(a) to connect the two couplers with enough space to avoid interference between the circuit components. Increasing the tilt improves the insertion loss and increases the matching bandwidth. The phase variations between the two ports must be considered, as this line and the transitions must have a 45° phase difference within the operating band. As will be seen later, the current line provides a larger-than-needed phase difference. However, this cannot be improved by changing the line length because its physical length must be kept constant. With this constraint, the phase difference can be changed by inserting open-circuit (OC) stubs to control the phase variation with frequency [54, 55]. Two multi-stage OC stubs are added to the line to decrease the phase difference. The OC stubs have a tapered end to allow a wideband of operation, as shown in Figure 5.8(b). The stubs delay the overall structure and decrease the phase difference between the line and multilayer transitions, as depicted in Figure 5.8(c).

Furthermore, an elliptical pad can be added at the end of the line in the multilayer transition to shift the phase difference with more flexibility [56]. The circular slot radius is fixed at 1.3 mm. The elliptic pad has a minor axis radius = 0.3 mm, and the major axis radius is varied. Figure 5.9 shows the S-parameters of the transition with various major axis radii. The phase difference is more stable over the band with a major axis radius > 0.8 mm. Therefore, the major axis radius of 0.93 mm achieves the 45° phase shift with $\pm$ 3° variation.

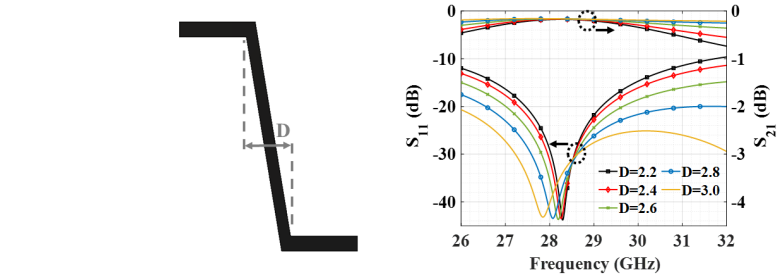

(a)

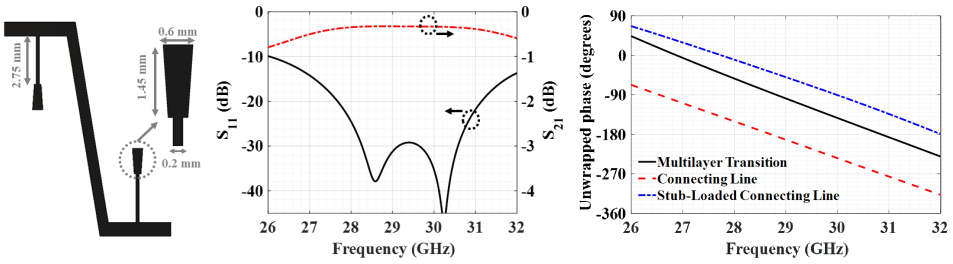

(b) (c)

Figure 5.8: (a) Effect of tilt (D) on couplers connecting line, (b) Couplers connecting line with multi-stage stubs, and (c) Phase variation of the multilayer and coupler connecting lines

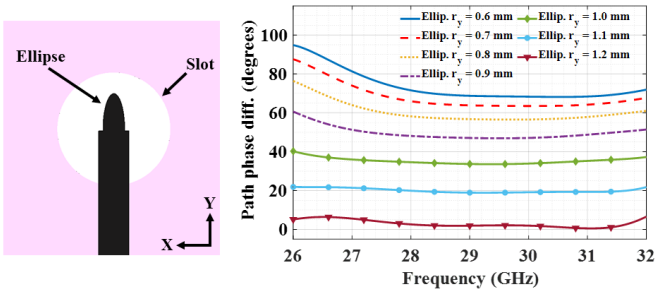

Figure 5.9: Effect of changing the ellipse r_y on the path phase difference between the multilayer transition and couplers connecting line

5.2.5 Slot Antenna

To ensure that each port possesses the same phase behavior and to decrease complexity, a multilayer transition is used to bring all the signals to the lower layer to permit using one antenna. Slot antennas are characterized by their compact structure, wideband of operation, and ability to be backed easily by an AMC to suppress direct back radiation [57, 58]. To couple the signal from the bottom layer to the upper layer, a circular slot with a radius of 1.7 mm is used to couple to a rectangular cavity with a radiating rectangular slot at the top. The rectangular slot has a length of 5.6 mm and a width of 2.5 mm, as shown in Figure 5.10. This type of orientation allows the antenna to be integrated directly with the BM without needing external transitions to miniaturize the whole structure further. The antenna displays wideband operation with a gain level better than 5.4 dB. The cross-polarization level is low within the band of operation, with the E-plane cross-polarization level less than -30 dB. The average 3-dB beamwidth in the H- and E-planes is 80° and 120°, respectively.

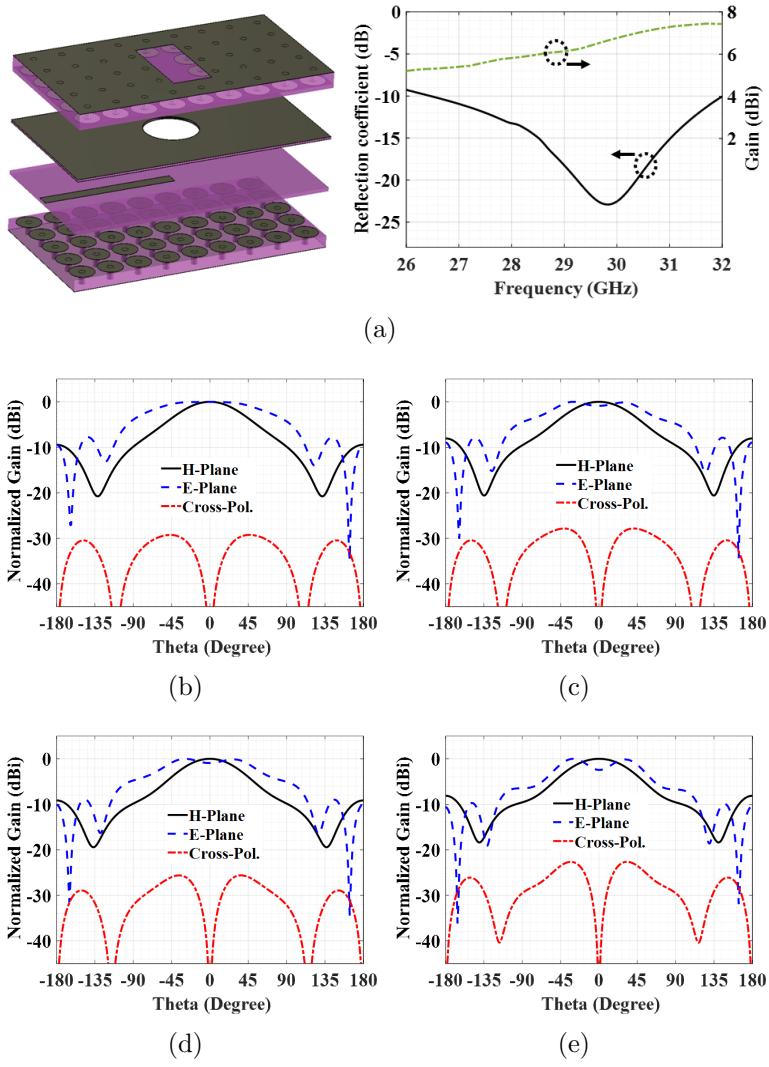

Figure 5.10: (a) Multilayer slot antenna and its frequency response, 2-D radiation patterns at (b) 27 GHz, (c) 28 GHz, (d) 29 GHz, and (e) 30 GHz

5.2.6 Components Integration

A folded 4 × 4 BM is constructed from the previously designed components, as shown in Figure 5.11. It is comprised of four quadrature hybrid couplers, two multilayer transitions, and two stub-loaded connecting lines. The 45° phase shift is carried out simultaneously at the multilayer transitions with respect to the stub-loaded connecting lines. The final structure is realized by folding the top layer around the folding line and AMC packaging the whole structure from the top and bottom. Port alignment is simply implemented, as ports #6 and #7 are on different layers.

Due to the symmetry of the BM structure, it is sufficient to analyze only two inputs representing any (1X) and (2X) beams. As a result, input Port 1 (1R) and Port 3 (2R) are chosen to show the excitation for both layers. Both ports' scattering parameters and phase distribution are presented in Figure 5.12. The BM displays stable performance within the 27-31 GHz range. The insertion loss is 0.6 dB at the center frequency, with a variation of ±1.4 dB over the bandwidth. The input port isolation level is better than 14 dB, and the phase variation for both ports is around ±8°.

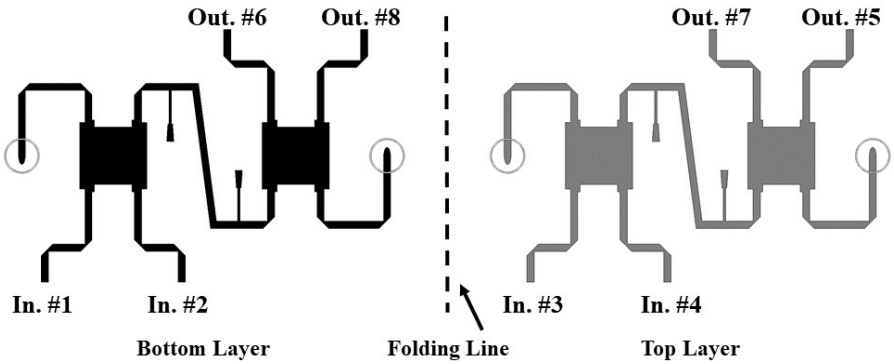

Figure 5.11: Realized folded 4 × 4 BM

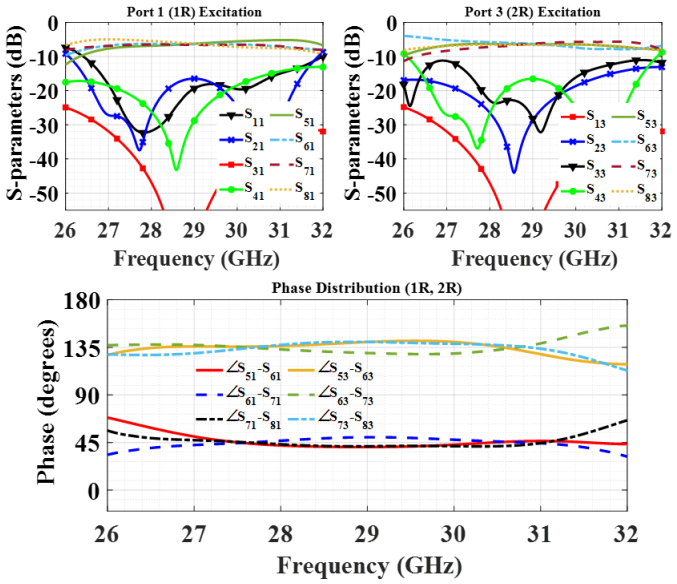

Figure 5.12: Scattering parameters and phase distribution for input Ports 1 (1R) and 3 (2R)

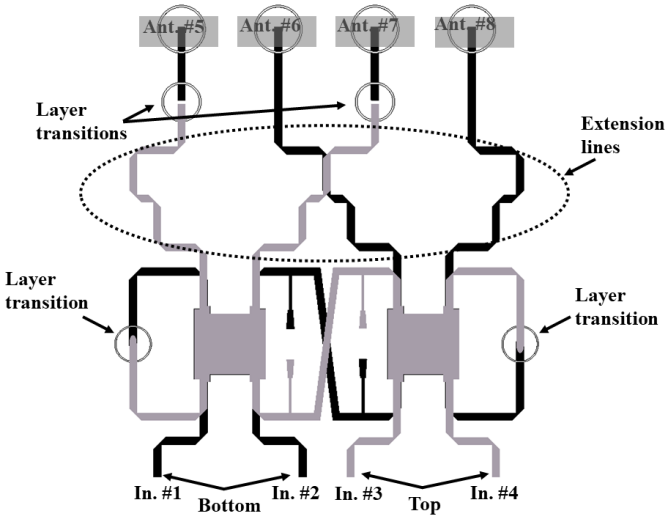

Figure 5.13: Full folded 4 × 4 BM with slot antennas (Planar view)

Figure 5.13 depicts the fully assembled BM with the slot antenna in a planar view, showing the multilayer transitions and extension lines. The extension lines align the output ports with two additional multilayer transitions to unite the antenna array's output layer. The full AMC packaged circuit is presented in Fig-

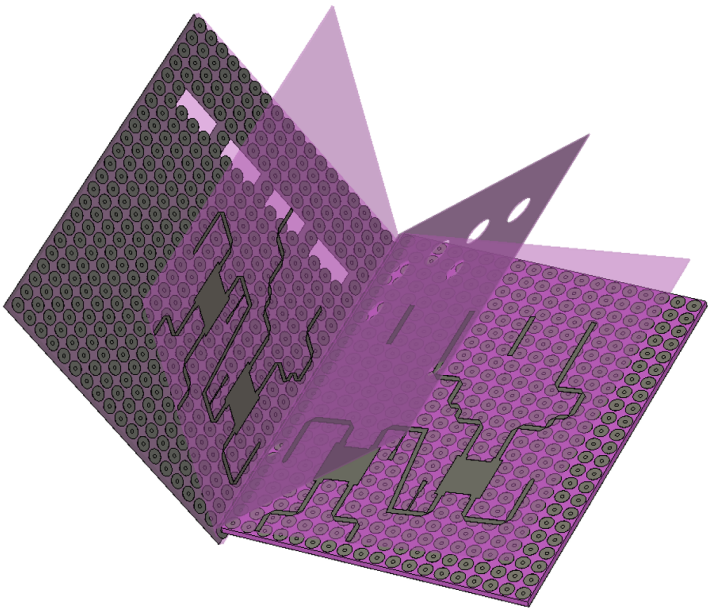

Figure 5.14: AMC packaged BM with slot antennas (Exploded view)

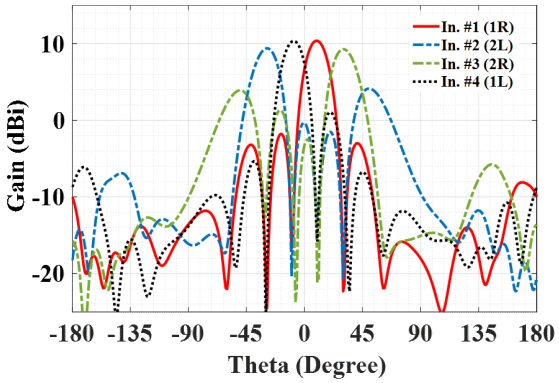

Figure 5.15: BM radiation patterns at 29 GHz

ure 5.14, showing each layer of the BM. Each port is excited to plot the far-field radiation patterns at 29 GHz, as shown in Figure 5.15. The beams are switched at θ = -30.5°, -9°, +9°, and +30.5°, with a gain of 10.37 dBi. The scan loss is less than 1 dB, with a cross-polarization level below -20 dB.

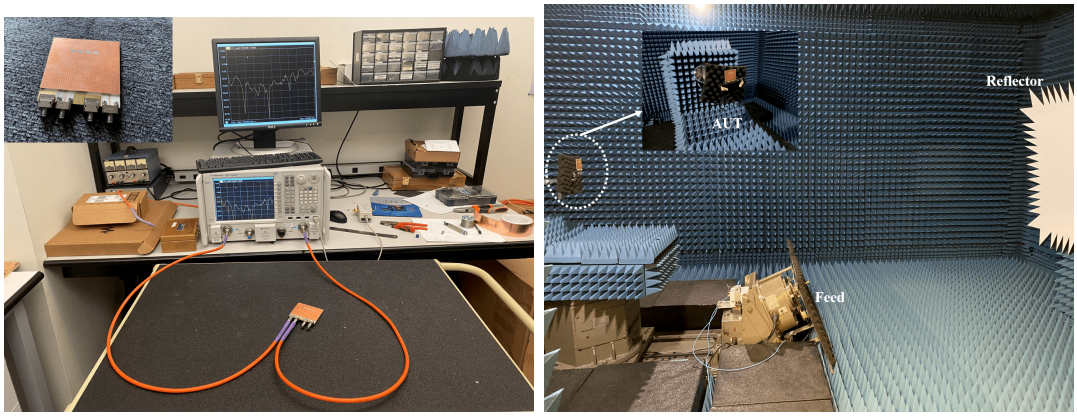

(a) (b)

Figure 5.16: (a) Fabricated BM and S-parameters measurements and (b) Far-field radiation pattern measurement

5.3 Measurements and Comparison

The multilayer BM is fabricated using standard PCB laser prototyping technology. Prepreg is inserted between the layers at the corners and in places distant from wave propagation. All the layers are aligned and stacked, then exposed to high temperatures and pressed together to form a multilayer board. This eliminates accidental air gaps and ensures a solid and stable PCB for measurement. The fabricated prototype and measurement setups are displayed in Figure 5.16.

The simulated and measured scattering parameters and gain of the multi-beam antenna prototype are shown in Figure 5.17. As the network is symmetric, only the results for beam Ports 1 (1R) and 3 (2R) are presented. A bandwidth of 4 GHz (27–31 GHz) is maintained for both ports, with beam port isolation better than 14 dB. The maximum gain values for beam ports 1R and 2R are 10.41 and 9.5 dBi, respectively. The gain is measured in comparison to the standard horn gain. The measured and simulated results are in good agreement. The slight shift in the measured result and dip in the gains could result from fabrication tolerance

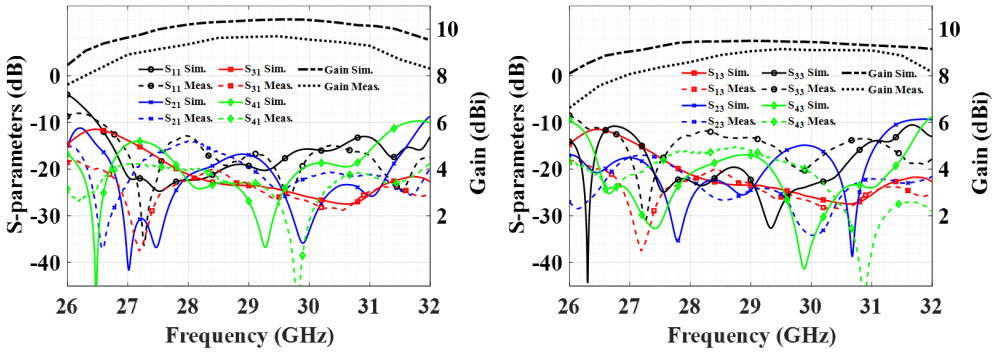

(a) (b)

Figure 5.17: Measured and simulated scattering parameters of BM and gain of the antenna arrays at Input (a) Port 1 and (b) Port 3

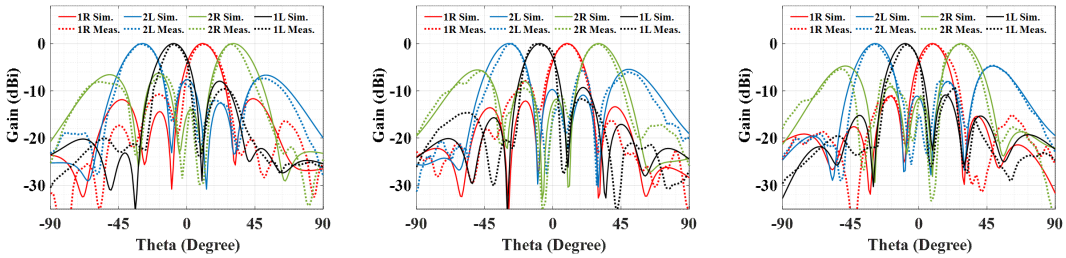

(a) (b) (c)

Figure 5.18: Measured and simulated radiation patterns at (a) 28 GHz, (b) 29 GHz, and (c) 30 GHz

and alignment imperfections. Moreover, the adhesive over the propagation paths can slightly affect the effective permittivity.

Figure 5.18 displays the measured normalized radiation patterns in comparison to the simulated patterns at frequencies of 28, 29, and 30 GHz. At 29 GHz, beams are switched at ±9° and ±30.5°, with a maximum gain of 10.37 and 9.5 dBi and the crossing points at -3.4 and -4 dB, respectively. The adjacent beams are 21.5° apart. A good agreement between the simulation and the measured beam-switching performance is observed.

Table 5.1 compares the presented work with other recent related work in terms

Table 5.1: Comparison between different BMs configurations in the literature

Reference	Layout	BW%@f_0 (GHz)	Isolation (dB)	Size (λ^2)
[27]	Planar	16.7%@30	≥15	4.16 × 3.64
[59]	Planar	21.2%@30	≥13	9 × 5.4
[60]	Planar	7.8%@25.5	≥11	3.21 × 3.2
[61]	Multilayer	N/A%@28	N/A	1.7 × 2.1
[62]	Multilayer	N/A%@28	N/A	1.31 × 1.87
This work	**Multilayer**	**13.8%@29**	**≥14**	**3.49 × 2.2**

of design layout, impedance bandwidth, port isolation, and overall size (excluding antennas). In [27], a planar MSL BM is packaged using metallic pins from the top and bottom with horn antennas, creating an overall bulky design when the metallic housing is considered. PRGW is used in [59] to design a packaged BM with a wideband operation. However, this comes at the cost of having a very large structure. The substrate-integrated suspended line (SISL) packaging layout in [60] offers a compact structure at mmWave bands. However, multiple layers were used to package a planar structure with a narrow bandwidth and low isolation level. In [61] and [62], multilayer BMs are realized using microstrip and low-temperature co-fired ceramics (LTCC) technologies, respectively, with an extremely compact design. However, the design has a limitation of narrow bandwidth, whereas the presented design of a 4 × 4 BM covers a wideband of operation at the Ka-band. Additionally, AMC packaging ensures the suppression of radiation losses and shields the overall structure. Furthermore, it provides good matching and isolation levels where a wider band of operation is possible at the cost of more complicated components and a slightly less compact structure. The miniaturizing layout could also be applied to higher-order N × N BMs.

5.4 Summary

Different multilayer layouts have been presented to miniaturize N × N BMs. Components operating in the mmWave band have been designed and integrated to fit the 4 × 4 multilayer layouts to verify the concept. AMC packaging has suppressed radiation losses and created a self-packaged/shielded circuit. The multilayer layout reduced the size by more than half of the planar BM. At the center frequency, the insertion loss was 0.6 dB, and the isolation and matching levels were below 14 dB, with stable performance for a 13.8% bandwidth. Multilayer slot antennas are integrated into the BM, and a prototype for the beamforming network has been developed to validate the circuit.

Chapter 6

Conclusion and Future Work

This thesis has presented novel multilayer microwave devices to miniaturize their typical size and also provided a study of the EBG cell and methods for size reduction.

In Chapter 3, the operation of the EBG cell and parameters affecting the band-gap are described. The band-gap of the traditional cell could be shifted down by shifting the via to maximize the current path. Furthermore, a spiral-shaped EBG cell with its via shifted at the edge has been designed to lower the operating frequency while maintaining the same compact structure. The proposed spiral EBG cell has reduced its size significantly compared to a traditional cell with the same starting stopband's lower frequency.

Chapter 4 has presented MSL multilayer power dividers with wideband operation in the Ka-band. The power divider layout could be modified to achieve phase differences ranging from in- to out-of-phase output ports. The circuit has been packaged with an AMC for efficient packaging to suppress possible leakage. Better than 15 dB return loss has been realized with the required output phase difference of $\pm 6^{\circ}$ within 21.8% bandwidth.

Different multilayer layouts have been presented to miniaturize BMs for N x N sizes in Chapter 5. Components operating in the mmWave band have been designed and integrated to fit the 4 × 4 multilayer layout to verify the concept. AMC packaging has been used to suppress radiation losses and create a self-packaged/shielded circuit. The multilayer layout reduced the size by more than half of that in a planar format. At center frequency, the insertion loss is 0.6 dB, and the isolation and matching levels are below 14 dB, with stable performance for a 13.8% bandwidth. Multilayer slot antennas are integrated into the BM, and a prototype for the beamforming network has been developed to validate the circuit.

6.1 Future Work

A multilayer ultra-wideband phase shifter could be designed to improve the bandwidth of the multilayer BM. Also, other microwave devices could be implemented using the multilayer AMC packaged layout to reduce their sizes.

6.1.1 8 × 8 Multilayer Butler Matrix

The alternative layout in Figure 5.3(c) can be designed with the same components used in the 4 × 4 folded BM, in addition to other similar components. The realized multilayer 8 × 8 BM layout is presented in Figure 6.1(a). Furthermore, the crossover coupler can be laid out horizontally to reduce the overall size further, as shown in Figure 6.1(b). The additional components required to construct the overall 8 × 8 BM are depicted in Figure 6.2. The realized multilayer 8 × 8 BM structure using the components is presented in Figure 6.3. Finally, the frequency

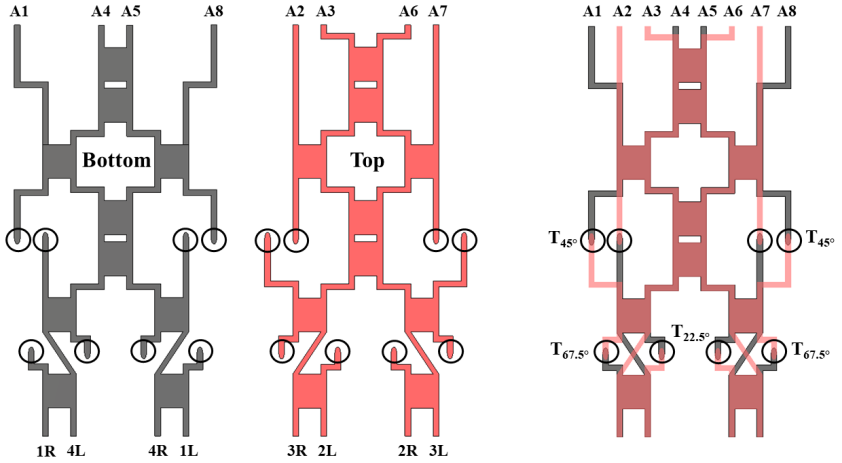

(a)

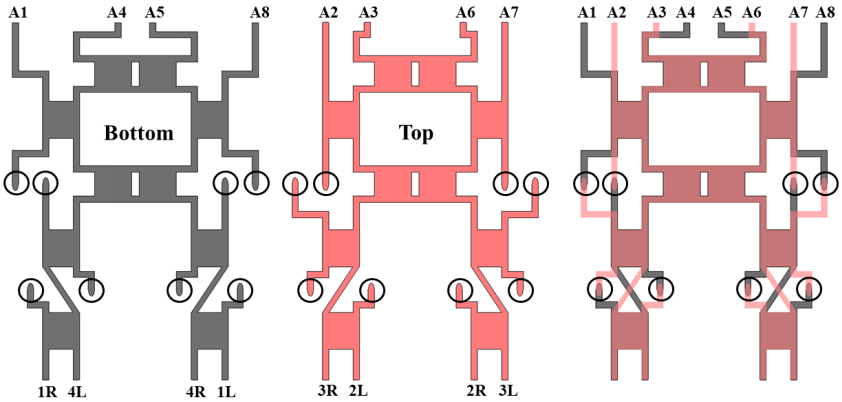

(b)

Figure 6.1: Multilayer 8 × 8 BM (Planar view) (a) Crossover couplers in vertical layout and (b) Crossover couplers in horizontal layout

response of the overall multilayer 8 × 8 BM is shown in Figure 6.4. Further work can be done to improve the amplitude and phase variations to achieve a wider bandwidth.

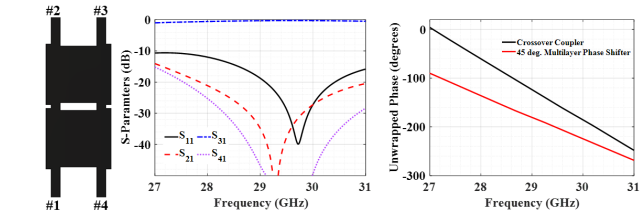

(a)

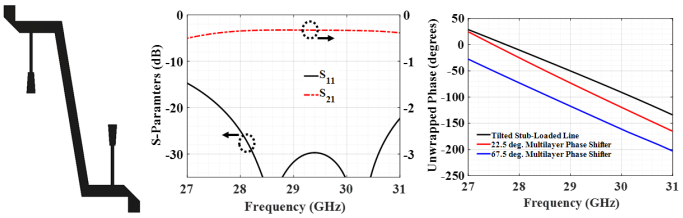

(b)

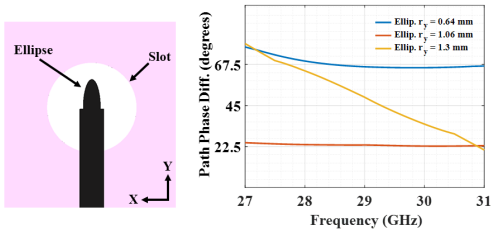

(c)

Figure 6.2: Multilayer 8 × 8 BM components (a) Crossover coupler, (b) Tilted stub-loaded line, and (c) Multilayer phase shifter

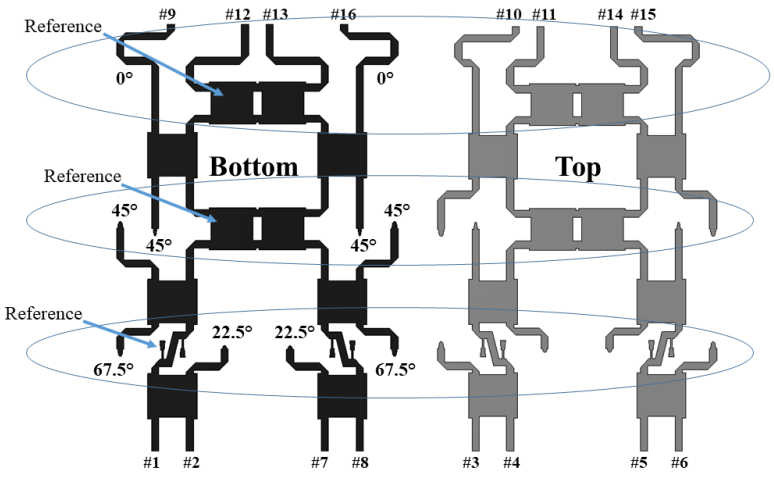

Figure 6.3: Realized multilayer 8 × 8 BM

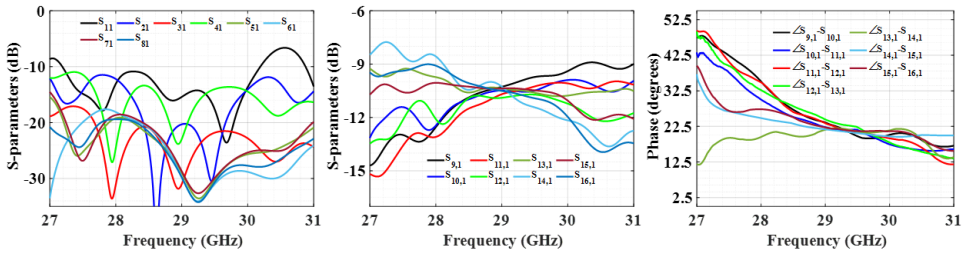

(a)

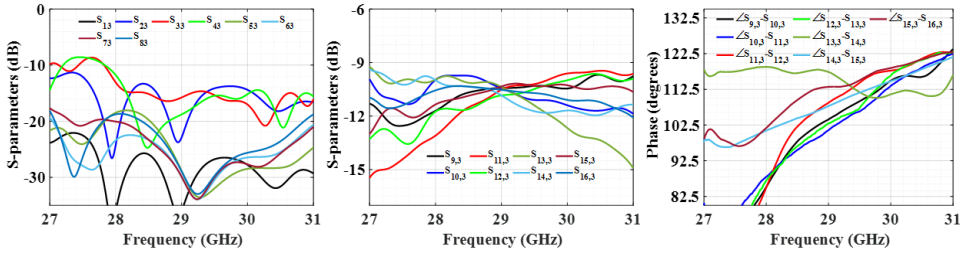

(b)

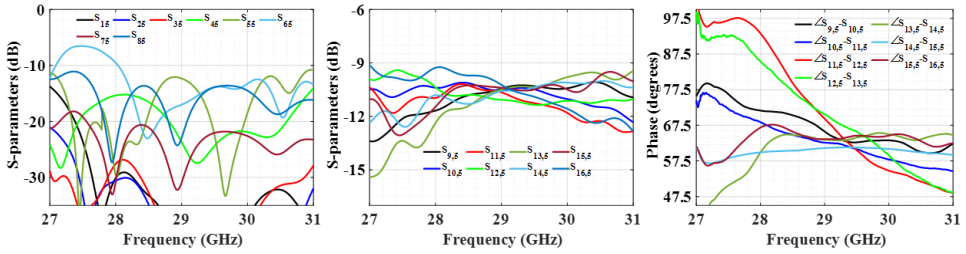

(c)

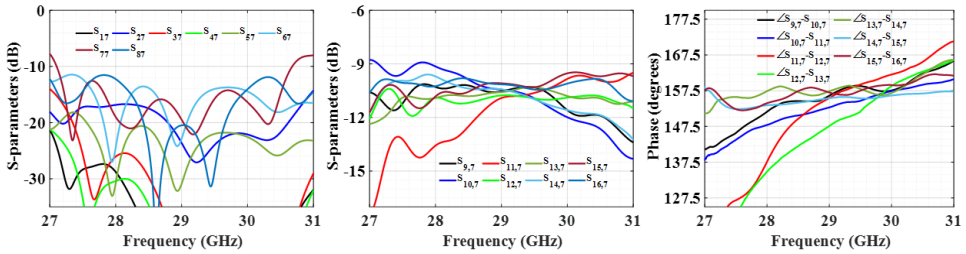

(d)

Figure 6.4: Multilayer 8 × 8 BM frequency response (a) Input 1 (1R), (b) Input 3 (3R), (c) Input 5 (2R), and (d) Input 7 (4R)

References

[1] C.-X. Wang *et al.*, "Cellular architecture and key technologies for 5G wireless communication networks," *IEEE Communications Magazine*, vol. 52, no. 2, pp. 122–130, 2014.

[2] E. Dahlman, S. Parkvall, and J. Skold, *5G NR: The next generation wireless access technology*. Academic Press, 2020.

[3] K.-C. Huang and D. J. Edwards, *Millimeter wave antennas for Gigabit wireless communications: a practical guide to design and analysis in a system context*. John Wiley & Sons, 2008.

[4] D. Grieg and H. Engelmann, "Microstrip-A new transmission technique for the Kilomegacycle range," *Proceedings of the IRE*, vol. 40, no. 12, pp. 1644–1650, 1952.

[5] R. N. Simons, *Coplanar waveguide circuits, components, and systems*. John Wiley & Sons, 2004.

[6] P.-S. Kildal, "Definition of artificially soft and hard surfaces for electromagnetic waves," *Electronics Letters*, vol. 24, pp. 168–170, 1988.

[7] P.-S. Kildal and A. Kishk, "EM modeling of surfaces with STOP or GO characteristics–artificial magnetic conductors and soft and hard surfaces,"

The Applied Computational Electromagnetics Society Journal (ACES), pp. 32–40, 2003.

[8] D. Sievenpiper, L. Zhang, R. F. Broas, N. G. Alexopolous, and E. Yablonovitch, "High-impedance electromagnetic surfaces with a forbidden frequency band," *IEEE Transactions on Microwave Theory and Techniques*, vol. 47, no. 11, pp. 2059–2074, 1999.

[9] P.-S. Kildal, "Three metamaterial-based gap waveguides between parallel metal plates for mm/submm waves," in *2009 3rd European Conference on Antennas and Propagation*, 2009, pp. 28–32.

[10] M. M. M. Ali, S. I. Shams, and A.-R. Sebak, "Printed ridge gap waveguide 3-dB coupler: Analysis and design procedure," *IEEE Access*, vol. 6, pp. 8501–8509, 2017.

[11] S Birgermajer, N Janković, V Crnojević-Bengin, M Bozzi, and V Radonić, "Forward-wave 0 dB directional coupler based on microstrip-ridge gap waveguide technology," in *2017 13th International Conference on Advanced Technologies, Systems and Services in Telecommunications (TELSIKS)*, 2017, pp. 154–157.

[12] M. M. M. Ali and A. Sebak, "Compact printed ridge gap waveguide crossover for future 5G wireless communication system," *IEEE Microwave and Wireless Components Letters*, vol. 28, no. 7, pp. 549–551, 2018.

[13] D. Shen, K. Wang, and X. Zhang, "A substrate integrated gap waveguide based wideband 3-dB coupler for 5G applications," *IEEE Access*, vol. 6, pp. 66 798–66 806, 2018.

[14] M. M. Mahmoud Ali, S. I. Shams, and A. Sebak, "Ultra-wideband printed ridge gap waveguide hybrid directional coupler for millimeter wave applications," *IET Microwaves, Antennas & Propagation*, vol. 13, no. 8, pp. 1181–1187, 2019.

[15] M. A. Abbas, M. F. Cengiz, A. Allam, D. E. Fawzy, H. M. Elhennawy, and M. F. A. Sree, "A novel circular reconfigurable metasurface-based compact UWB hybrid coupler for Ku-band applications," *IEEE Access*, vol. 10, pp. 129 781–129 790, 2022.

[16] M. S. Sorkherizi and A. A. Kishk, "Transition from microstrip to printed ridge gap waveguide for millimeter-wave application," in *2015 IEEE International Symposium on Antennas and Propagation & USNC/URSI National Radio Science Meeting*, 2015, pp. 1588–1589.

[17] J. Zhang, X. Zhang, D. Shen, and A. A. Kishk, "Packaged microstrip line: A new quasi-TEM line for microwave and millimeter-wave applications," *IEEE Transactions on Microwave Theory and Techniques*, vol. 65, no. 3, pp. 707–719, 2016.

[18] J.-S. Lim, S.-W. Lee, C.-S. Kim, J.-S. Park, D. Ahn, and S. Nam, "A 4.1 unequal Wilkinson power divider," *IEEE Microwave and Wireless Components Letters*, vol. 11, no. 3, pp. 124–126, 2001.

[19] K. W. Eccleston and S. H. Ong, "Compact planar microstripline branch-line and rat-race couplers," *IEEE Transactions on Microwave Theory and Techniques*, vol. 51, no. 10, pp. 2119–2125, 2003.

[20] M. Bialkowski and A. Abbosh, "Design of a compact UWB out-of-phase power divider," *IEEE Microwave and Wireless Components Letters*, vol. 17, no. 4, pp. 289–291, 2007.

[21] J. He, B.-Z. Wang, Q.-Q. He, Y.-X. Xing, and Z.-L. Yin, "Wideband X-band microstrip Butler matrix," *Progress In Electromagnetics Research*, vol. 74, pp. 131–140, 2007.

[22] C. H. Chen, H. Wu, and W. Wu, "Design and implementation of a compact planar 4 x 4 microstrip Butler matrix for wideband application," *Progress In Electromagnetics Research C*, vol. 24, pp. 43–55, 2011.

[23] B. Schiffman, "A new class of broad-band microwave 90-degree phase shifters," *IRE Transactions on Microwave Theory and Techniques*, vol. 6, no. 2, pp. 232–237, 1958.

[24] M. S. Sorkherizi and A. A. Kishk, "Fully printed gap waveguide with facilitated design properties," *IEEE Microwave and Wireless Components Letters*, vol. 26, no. 9, pp. 657–659, 2016.

[25] ——, "Self-packaged, low-loss, planar bandpass filters for millimeter-wave application based on printed gap waveguide technology," *IEEE Transactions on Components, Packaging and Manufacturing Technology*, vol. 7, no. 9, pp. 1419–1431, 2017.

[26] N. Ashraf, A. A. Kishk, and A. Sebak, "Broadband millimeter-wave beamforming components augmented with AMC packaging," *IEEE Microwave and Wireless Components Letters*, vol. 28, no. 10, pp. 879–881, 2018.

[27] N. Ashraf, A.-R. Sebak, and A. A. Kishk, "PMC packaged single-substrate 4× 4 Butler matrix and double-ridge gap waveguide horn antenna array

for multibeam applications," *IEEE Transactions on Microwave Theory and Techniques*, vol. 69, no. 1, pp. 248–261, 2020.

[28] M. M. M. Ali, M. S. El-Gendy, M. Al-Hasan, I. B. Mabrouk, A. Sebak, and T. A. Denidni, "A systematic design of a compact wideband hybrid directional coupler based on printed RGW technology," *IEEE Access*, vol. 9, pp. 56 765–56 772, 2021.

[29] Y. Wang, A. M. Abbosh, and B. Henin, "Broadband microwave crossover using combination of ring resonator and circular microstrip patch," *IEEE Transactions on Components, Packaging and Manufacturing Technology*, vol. 3, no. 10, pp. 1771–1777, 2013.

[30] A. Abbosh and M. Bialkowski, "Design of ultra wideband 3dB quadrature microstrip/slot coupler," *Microwave and Optical Technology Letters*, vol. 49, no. 9, pp. 2101–2103, 2007.

[31] A. M. Abbosh, "Ultra-wideband phase shifters," *IEEE Transactions on Microwave Theory and Techniques*, vol. 55, no. 9, pp. 1935–1941, 2007.

[32] A. Abbosh, "Ultra wideband inphase power divider for multilayer technology," *IET Microwaves, Antennas & Propagation*, vol. 3, no. 1, pp. 148–153, 2009.

[33] M. Traii, M. Nedil, A. Gharsallah, and T. A. Denidni, "A novel wideband Butler matrix using multi-layer technology," *Microwave and Optical Technology Letters*, vol. 51, no. 3, pp. 659–663, 2009.

[34] X.-C. Ji, W.-S. Ji, L.-Y. Feng, Y.-Y. Tong, and Z.-Y. Zhang, "Design of a novel multi-layer wideband bandpass filter with a notched band," *Progress In Electromagnetics Research Letters*, vol. 82, pp. 9–16, 2019.

[35] M. Farahani, M. Akbari, M. Nedil, T. A. Denidni, and A. R. Sebak, "A novel low-loss millimeter-wave 3-dB 90° ridge-gap coupler using large aperture progressive phase compensation," *IEEE Access*, vol. 5, pp. 9610–9618, 2017.

[36] M. M. M. Ali, O. M. Haraz, I. Afifi, A.-R. Sebak, and T. A. Denidni, "Ultra-wideband compact millimeter-wave printed ridge gap waveguide directional couplers for 5G applications," *IEEE Access*, vol. 10, pp. 90 706–90 714, 2022.

[37] A. T. Hassan, M. A. M. Hassan, and A. A. Kishk, "Modeling and design empirical formulas of microstrip ridge gap waveguide," *IEEE Access*, vol. 6, pp. 51 002–51 010, 2018.

[38] S. I. Shams and A. A. Kishk, "Printed texture with triangle flat pins for bandwidth enhancement of the ridge gap waveguide," *IEEE Transactions on Microwave Theory and Techniques*, vol. 65, no. 6, pp. 2093–2100, 2017.

[39] M. O. Shady and A. M. M. A. Allam, "A novel design of printed ridge gap waveguide-based 0-dB backward-wave coupler," *International Journal of RF and Microwave Computer-Aided Engineering*, vol. 32, no. 11, e23386, 2022.

[40] A. U. Zaman, V. Vassilev, P.-S. Kildal, and A. Kishk, "Increasing parallel plate stop-band in gap waveguides using inverted pyramid-shaped nails for slot array application above 60GHz," in *Proceedings of the 5th European Conference on Antennas and Propagation (EUCAP)*, 2011, pp. 2254–2257.

[41] E. Rajo-Iglesias, P.-S. Kildal, A. U. Zaman, and A. Kishk, "Bed of springs for packaging of microstrip circuits in the microwave frequency range," *IEEE Transactions on Components, Packaging and Manufacturing Technology*, vol. 2, no. 10, pp. 1623–1628, 2012.

[42] E. Rajo-Iglesias, E. Pucci, A. A. Kishk, and P.-S. Kildal, "Suppression of parallel plate modes in low frequency microstrip circuit packages using lid of printed zigzag wires," *IEEE Microwave and Wireless Components Letters*, vol. 23, no. 7, pp. 359–361, 2013.

[43] C.-L. Wang, G.-H. Shiue, W.-D. Guo, and R.-B. Wu, "A systematic design to suppress wideband ground bounce noise in high-speed circuits by electromagnetic-bandgap-enhanced split powers," *IEEE Transactions on Microwave Theory and Techniques*, vol. 54, no. 12, pp. 4209–4217, 2006.

[44] T. Kamgaing and O. M. Ramahi, "Multiband electromagnetic-bandgap structures for applications in small form-factor multichip module packages," *IEEE Transactions on Microwave Theory and Techniques*, vol. 56, no. 10, pp. 2293–2300, 2008.

[45] M. S. Sorkherizi, A. Dadgarpour, and A. A. Kishk, "Planar high-efficiency antenna array using new printed ridge gap waveguide technology," *IEEE Transactions on Antennas and Propagation*, vol. 65, no. 7, pp. 3772–3776, 2017.

[46] M. M. M. Ali and A. Sebak, "Printed RGW circularly polarized differential feeding antenna array for 5G communications," *IEEE Transactions on Antennas and Propagation*, vol. 67, no. 5, pp. 3151–3160, 2019.

[47] J. L. Butler, *Multiple beam antenna system employing multiple directional couplers in the leadin*, US Patent 3 255 450, Jun. 7, 1966.

[48] H. J. Chaloupka, "Application of high-temperature superconductivity to antenna arrays with analog signal processing capability," in *1994 24th European Microwave Conference*, vol. 1, 1994, pp. 23–35.

[49] A. Corona and M. Lancaster, "A high-temperature superconducting Butler matrix," *IEEE Transactions on Applied Superconductivity*, vol. 13, no. 4, pp. 3867–3872, 2003.

[50] J.-S. Néron and G.-Y. Delisle, "Microstrip EHF Butler matrix design and realization," *ETRI journal*, vol. 27, no. 6, pp. 788–797, 2005.

[51] H Moody, "The systematic design of the Butler matrix," *IEEE Transactions on Antennas and Propagation*, vol. 12, no. 6, pp. 786–788, 1964.

[52] T. Kawai and I. Ohta, "Planar-circuit-type 3-dB quadrature hybrids," *IEEE Transactions on Microwave Theory and Techniques*, vol. 42, no. 12, pp. 2462–2467, 1994.

[53] S. Y. Zheng, S. H. Yeung, W. S. Chan, K. F. Man, and S. H. Leung, "Size-reduced rectangular patch hybrid coupler using patterned ground plane," *IEEE Transactions on Microwave Theory and Techniques*, vol. 57, no. 1, pp. 180–188, 2008.

[54] S. Y. Zheng, W. S. Chan, and K. F. Man, "Broadband phase shifter using loaded transmission line," *IEEE Microwave and Wireless Components Letters*, vol. 20, no. 9, pp. 498–500, 2010.

[55] K. Ding and A. A. Kishk, "2-D Butler matrix and phase-shifter group," *IEEE Transactions on Microwave Theory and Techniques*, vol. 66, no. 12, pp. 5554–5562, 2018.

[56] L Guo and A Abbosh, "Phase shifters with wide range of phase and ultra-wideband performance using stub-loaded coupled structure," *IEEE Microwave and Wireless Components Letters*, vol. 24, no. 3, pp. 167–169, 2014.

[57] S. M. Sifat, M. M. M. Ali, S. I. Shams, and A.-R. Sebak, "High gain bow-tie slot antenna array loaded with grooves based on printed ridge gap waveguide technology," *IEEE Access*, vol. 7, pp. 36 177–36 185, 2019.

[58] H. Attia, A. A. Kishk, M. A. Abdalla, S. Gaya, A. Hamza, and A. Mahmoud, "Ridge gap waveguide antenna array with improved mutual isolation for millimeter wave applications," *International Journal of RF and Microwave Computer-Aided Engineering*, vol. 31, no. 11, e22831, 2021.

[59] I. Afifi and A.-R. Sebak, "Wideband 4× 4 Butler matrix in the printed ridge gap waveguide technology for millimeter-wave applications," *IEEE Transactions on Antennas and Propagation*, vol. 68, no. 11, pp. 7670–7675, 2020.

[60] Y. Wang, K. Ma, and Z. Jian, "A low-loss Butler matrix using patch element and honeycomb concept on SISL platform," *IEEE Transactions on Microwave Theory and Techniques*, vol. 66, no. 8, pp. 3622–3631, 2018.

[61] S. Kim, S. Yoon, Y. Lee, and H. Shin, "A miniaturized Butler matrix based switched beamforming antenna system in a two-layer hybrid stackup substrate for 5G applications," *Electronics*, vol. 8, no. 11, p. 1232, 2019.

[62] S. Nam, S. Choi, J. Ryu, and J. Lee, "Compact 28 GHz folded Butler matrix using low-temperature co-fired ceramics," *Journal of Electromagnetic Engineering and Science*, vol. 22, no. 4, pp. 452–458, 2022.